2019-06-15

Stratigraphic and environmental control on marine benthic community change through the early Toarcian extinction event (Iberian Range, Spain)

Danise, Silvia

10.1016/j.palaeo.2019.03.039
Palaeogeography, Palaeoclimatology, Palaeoecology
Elsevier

Stratigraphic and environmental control on marine benthic community change through the early Toarcian extinction event (Iberian Range, Spain)

Silvia Danise[1*], Marie-Emilie Clémence[2], Gregory D. Price[2], Daniel P. Murphy[3], Juan J. Gómez[4], and Richard J. Twitchett[5]

[1]Università degli Studi di Firenze, Dipartimento di Sicenze della Terra, via La Pira 4, 50121, Firenze, Italy

[2]School of Geography, Earth and Environmental Sciences, University of Plymouth, Drake Circus, Plymouth, Devon PL4 8AA UK.

[3]Eastfiled College, Dallas County Community College District, 3737 Motley Drive, Mesquite, TX 75150, USA.

[4]Departamento de Geodinámica, Estratigrafía y Paleontología, Facultad de Cuancias Geológicas (UCM) and Instituto de Geociencias (CSIC-UCM), c/ Jose Antonio Novais, 12. 28040 Madird, Spain.

[5]Department of Earth Sciences, Natural History Museum, Cromwell Road, London, SW7 5BD, UK

[*] Corresponding author: silvia.danise@unifi.it

ABSTRACT

In the Early Jurassic (~183 Ma ago) global warming and associated environmental changes coincided with an extinction event in the marine realm (early Toarcian extinction event). Anoxia was previously considered to have been the main cause of extinction, but extinctions also occur at localities that remained oxygenated throughout the event, suggesting that other factors, such as temperature, may have played a major role. To test this hypothesis, we integrated quantitative analyses of benthic macro-invertebrates with high-resolution geochemical proxies on the bulk rock (TOC, $\delta^{13}C$, $\delta^{18}O$) and on brachiopod and belemnite shells ($\delta^{13}C$, $\delta^{18}O$) from two sections from the Iberian Range, Spain, with no black shale deposition. The sections are orientated SE-NW along an onshore-offshore gradient deepening to the north. The dominant benthic groups, bivalves and brachiopods, show a different response to the extinction: brachiopods go through a complete species-level turnover, while many bivalve species range through the event. In the shallower section, changes in richness and evenness correlate with TOC (Total Organic Carbon), suggesting that variations in nutrient input from runoff, and the possible local onset of low-redox conditions (TOC > 4 wt%), controlled faunal diversity. In contrast, at the deeper section, community change correlates with changes in $\delta^{18}O$, indicating that temperature variations might have influenced faunal change. Different stratigraphic patterns of extinction occur between the two localities, with last-occurrences clustering at the maximum flooding surface in the shallower section, and at the transgressive surface in the deeper one. The observed differences between the two localities highlight the important role of local sedimentary and stratigraphic processes in controlling the shape of the geochemical and fossil record, and the need for studying multiple sections along onshore-offshore gradients in order to extrapolate regional and global patterns.

Keywords: Jurassic, warming, anoxia, bivalves, brachiopods, stable isotopes

1. Introduction

Lower Jurassic (Pliensbachian-Toarcian, ~183 Ma) deposits record some of the most severe environmental perturbations of the Mesozoic. Pronounced (~2–5‰) negative carbon isotope excursions (CIEs) are recorded in marine carbonates and organic carbon from several sites around the world at the Pliensbachian/Toarcian boundary and at the *Tenuicostatum-Falciferum* Zone transition of the early Toarcian, suggesting a substantial input of isotopically light carbon into the atmosphere–ocean system (Hesselbo et al. 2000; 2007; Jenkyns et al. 2001; Kemp et al. 2005; Littler et al. 2010; Izumi et al. 2012), probably from volcanic activity (Burgess et al. 2015). In the early Toarcian, an increase in seawater temperature of ~4–7 °C has been inferred from belemnite Mg/Ca and $\delta^{18}O$ ratios from various European sections (McArthur et al. 2000; Bailey et al. 2003; Gómez and Goy 2011), and $\delta^{18}O$ of brachiopods shells from Peniche section, Portugal (Suan et al. 2008). Higher global temperatures may have accelerated the hydrological cycle and increased continental chemical weathering, elevating nutrient input to the shelf seas and oceans (Cohen et al. 2004; Jenkyns 2010). These conditions likely favoured higher primary organic productivity and organic matter fluxes, ultimately triggering anoxic to euxinic conditions in many epicontinental seas (Toarcian Oceanic Anoxic Event: T–OAE; Jenkyns 1988; 2010). Furthermore, massive pulses of CO_2 input are thought to have triggered a carbonate system crisis through associated ocean acidification (Suan et al. 2008; Trecalli et al. 2012; Brazier et al. 2015).

This time interval is also characterised by a second-order extinction event affecting both pelagic and benthic organisms (Little and Benton 1995; Cecca and Macchioni 2004; Caswell et al. 2009; García Joral et al. 2011; Caruthers et al. 2013; Danise et al. 2013; 2015; Martindale and Aberhan 2017; Dunhill

et al. 2018a). Anoxia has been considered the main cause of the marine extinction, as the event was firstly recognised in settings characterised by the deposition of widespread organic rich black shales (e.g., Little and Benton 1995). However, this hypothesis has been questioned following discovery that the extinction event is also recorded in localities that remained fully oxygenated throughout the lower Toarcian (Gómez and Goy 2011; García Joral et al. 2011; Arias 2013). In particular, the absence of black shale deposition in most of northern and central Spain has been used to support the hypothesis that temperature rise, and not anoxia, was the main trigger of extinction on a global scale (Gómez et al. 2008; Gómez and Goy 2011).

In order to better understand which factors controlled changes in marine benthic communities in the absence of widespread black shale deposition, we collected quantitative macro-invertebrate data from two sections of the Iberian Range, central Spain (Castrovido and Sierra Palomera). The study sites were selected because they record deposition at different water depths along an onshore-offshore gradient of the western Tethyan shelf, which enables us to better understand the role of sedimentary and stratigraphic processes on the distribution of fossils through the extinction event (i.e., Holland 2000; 2015, Nawrot et al. 2017). Furthermore, the presence of both bivalves and brachiopods at both study sites (Comas-Rengifo et al. 1988; 1996), enables us to test whether these different taxonomic groups responded differently to the same event and/or to the same environmental drivers or not, providing a test of the generality of faunal responses (e.g., Belanger 2012; Danise et al. 2015). For this purpose, faunal data were integrated with high-resolution geochemical proxies on the bulk rock (TOC, $\delta^{13}C$, $\delta^{18}O$) and on calcitic brachiopod and belemnite shells ($\delta^{13}C$, $\delta^{18}O$), to test for possible correlations between biotic and environmental change.

The main objectives of this study are: (1) to identify, through high-resolution chemostratigraphy, the Pliensbachian/Toarcian and early Toarcian events at the localities of Castrovido and Sierra

Palomera; (2) to analyse and compare the responses to the early Toarcian extinction event of two different taxonomic groups, bivalves and brachiopods; (3) to test how richness, evenness, and community composition of benthic macro-invertebrates correlate with variations in TOC, $\delta^{13}C$ and $\delta^{18}O$ from calcitic shells; (4) to evaluate the role of stratigraphic processes in shaping the distribution of species through the extinction event.

2. Geological and stratigraphic setting

The studied sections of Castrovido and Sierra Palomera are located in the Iberian Range, a NW trending fold- and thrust-belt in eastern Spain which formed during the Paleogene by inversion of Mesozoic rifted basins (Fig. 1A; Salas et al. 2001; Gómez and Fernández-López 2006). In the Late Triassic to Middle Jurassic the area comprised a system of shallow marine platforms of the western Tethys shelf that developed on the progressively submerging Iberian block, under a post-rift extensional tectonic regime (Fig. 1B; Gómez and Goy 2005). This platform system was connected eastward with the Tethyan Ocean, to the north with the Arctic, through the so-called Viking Corridor (Callomon 1979) or "Laurasian Seaway" (Bjerrum et al. 2001), and to the west with South America through the Hispanic Corridor, which had probably been intermittently open since the Sinemurian/Pliensbachian boundary (Aberhan 2001; Damborenea 2002; Martindale and Aberhan 2017).

At both study sites, the upper Pliensbachian is represented by the Barahona Limestone Formation, which consists mainly of lime wackestones to packstones, with occasional mudstone, skeletal grainstones and minor interbedded marls. The Barahona Limestone Formation formed in a high energy, shallow ramp, frequently influenced by storms (Gómez and Goy 2005). This formation spans the Pliensbachian *Margaritatus* and *Spinatum* ammonite zones (Comas-Rengifo 1985). However, due to synsedimentary tectonics, the top of the unit is diachronous, and in the central portion of the

southwestern branch of the Iberian Range its upper boundary is correlated with the lower Toarcian *Tenuicostatum* Zone (e.g., in the Sierra Palomera section; Comas-Rengifo et al. 1996). Deposition of the overlying Turmiel Formation began with the progressive deepening of the platform in the early Toarcian. This formation is characterized by an alternation of lime mudstones and marls deposited in a gently sloping, open-marine, homoclinal ramp (Gómez et al. 2003).

At both sections deposition took place below storm wave base (Comas-Rengifo et al. 1996). The progressive flooding of the platform culminated in a peak transgression in the mid-Toarcian *Bifrons* Zone (Quesada et al. 2005). Palaeogeographic reconstructions of the Western Tethys Iberian platform system, now cropping out along the Asturias, Basque–Cantabrian, Iberian and Catalonian basins, indicate that this ramp deepened and opened towards the north, changing from from inner to outer ramp settings (Aurell et al. 2003, Gómez and Goy 2005; Quesada et al. 2005). The Sierra Palomera section was thus deposited in shallower waters than Castrovido. Previous palaeocological studies on the benthic fauna estimated water depth to be about 40-70 m on average for a locality very close to the Sierra Palomera section (Gahr 2002; 2005).

From a sequence stratigraphic point of view, the early Jurassic Iberian Platform System has been subdivided into second and third order transgressive-regressive cycles (Fig. 2; Gómez and Goy 2005). The studied interval is part of the second order LJ3 cycle, and comprises the lower part of the LJ3-1 cycle, the entire LJ3-2 cycle (subdivided into two sub-cycles) and the lower part of the LJ3-3 cycle (Comas-Renfigo et al. 1988; 1996; Gómez and Goy 2005). Ammonite biostratigraphy is used for correlation, and follows Comas-Rengifo et al. (1996) and Osete et al. (2007) for the Sierra Palomera section, and Comas-Renfigo et al. (1988) and García Joral et al. (2011) for the Castrovido section.

3. Methods

133

134 *3.1. Sample collection*

135 At both sections, samples were collected for geochemical analysis and for palaeoecological
136 analysis of the fossil macro-invertebrates. At Castrovido, bulk rock samples were collected for $\delta^{13}C$,
137 $\delta^{18}O$ and TOC analyses with an average spacing of 10 cm (n=169; Table S1). At Sierra Palomera, bulk
138 rock samples for $\delta^{13}C$ and $\delta^{18}O$ analyses were collected at an average resolution of 11 cm (n=211; Table
139 S2), and TOC analyses at an average resolution of 26 cm (n=84; Table S2). From each fossiliferous bed,
140 belemnites and brachiopods were collected for stable isotope and trace element analysis. When
141 available, up to four specimens from the same bedding plane were analysed to assess the intra-horizon
142 variability of the geochemical data. A total of 50 belemnites and 33 brachiopods were analysed from the
143 Castrovido section (Table S1), 22 belemnites and 23 brachiopods from the Sierra Palomera section
144 (Table S2). The degree of diagenetic alteration of belemnite and brachiopod shells was assessed through
145 visual screening, cathodoluminescence analysis of thin sections, and trace elements analysis (see below).
146 At each site, from each fossiliferous bed, a standard mass of 2.5 kg of bulk rock was collected for the
147 quantitative analysis of benthic macro-invertebrates. A total of 76 bulk samples were collected (25 at
148 Castrovido; 51 at Sierra Palomera; Table S3).

149

150 *3.2. Cathodoluminescence analysis*

151 Cathodoluminescence (CL) analyses were performed with a CITL MK5 cathodoluminescence
152 instrument equipped with a Nikon microscope and digital camera at the University of Plymouth. CL is
153 widely employed as a screening technique that allows the identification of diagenetically altered shell
154 material (see however Barbin 2013 for a critical review of the method). The CL behaviour of marine
155 carbonates is a good indicator of burial diagenesis because many secondary calcites exhibit

luminescence that is activated by Mn^{2+}. As a result, non-luminescent biogenic carbonates are generally considered to be unaltered (e.g., Kearsey et al. 2009; Rosales et al. 2001). After screening, belemnites were classified into three classes: (1) well preserved and non-luminescent, with well-preserved microstructure (Fig. 3A); (2) moderately preserved, with rare microborings or microfractures and stylolites (Fig. 3B); and (3) poorly preserved, with extensive microborings, microfractures and stylolites (Fig. 3C). Class 3 belemnites and the diagenetically altered portions of Class 2 belemnites were excluded from the study. Only Class 1 belemnites and unaltered portions of Class 2 belemnites were sampled and analysed. The same classes were applied to brachiopod shells. Rhynchonellid brachiopod shells had the best-preserved microstructure, with most specimens exhibiting very low luminescence and only rare microfractures (Figs. 3D, E), whereas terebratulid shells have a porous shell structure characterized by endopunctae (Fig. 3F). Areas of brachiopod shells with cement- or matrix-filled endopunctae were excluded from the analysis.

3.3. Isotopes and trace element analysis

Using a microdrill, 0.3-0.5 mg of bulk rock from the fine fraction carbonate areas, avoiding any fossil material, was collected from each sample for trace element and isotope analysis. These carbonate powders were reacted with 100% phosphoric acid at 90°C, and the evolved CO_2 was analysed on a GV Instruments Isoprime mass spectrometer with a Gilson Multiflow carbonate autosampler at the University of Plymouth. The results were calibrated against the Vienna Peedee Belemnite (VPDB) using the international standard NBS-19 (National Bureau of Standards 19; $\delta^{13}C$=1.95‰ $\delta^{18}O$=−2.20‰). Reproducibility of replicate analyses for both $\delta^{18}O$ and $\delta^{13}C$ was better than 0.1‰.

Brachiopod shells were cleaned and sectioned longitudinally, while belemnites were cut perpendicular to the rostrum length. The outer (primary) layer of brachiopod shells is known to be in

isotopic disequilibrium (e.g., Parkinson et al. 2005), and so only secondary layers were sampled. Areas of the belemnite rostrum that are typically most prone to diagenesis (the rostrum exterior and the porous apical region) were avoided. A microdrill and an optical microscope were used to sample the best-preserved parts of the shells and rostra, as identified by CL and microscopy. Between 0.2 and 0.3 mg of carbonate powders were analysed for $\delta^{13}C$ and $\delta^{18}O$ using the same method as that used for the bulk rock analysis. Brachiopod and belemnite specimens were also sampled for trace elements (Mn and Fe). Sample powders were reacted with 0.2 M HNO_3 and measured at the University of Copenhagen using an Optima 7000 DV ICP-OES. Accuracy and analytical precision of the analyses were measured through interspersed aliquots of JLs-1 (Japanese limestone standard-1), which gave averages (±2 sd) of Fe/Ca = 0.062 ± 0.01 mmol/mol and Mn/Ca = 0.029 ± 0.006 mmol/mol. These results are in good agreement with published values giving averages (± 2 err) of Fe/Ca = 0.20 ± 0.1 mmol/mol, and Mn/Ca = 0.030 ± 0.004 mmol/mol (Imai et al. 1996). Inferred palaeotemperatures from $\delta^{18}O_{brac}$ and $\delta^{18}O_{bel}$ (Table S1 and S2) were calculated from the equation of Anderson and Arthur (1983), assuming an ice-free Jurassic world and a $\delta^{18}O_{seawater}$ of −1‰ V-SMOW (Shackleton and Kennett 1975).

3.4. Total organic carbon (TOC, wt%)

TOC analyses of the Sierra Palomera section were carried out on a SKALAR Primacs SLC. The instrument was calibrated and standards (Oxalic Acid) were run throughout to maintain precision of results. TOC analysis for the Castrovido samples were carried out at the National Oceanographic Centre, University of Southampton using a CHNOS analyser, with the BCSS-1 CRM standard, following the procedure of Nieuwenhuize et al. (1994). For both sets of analyses reproducibility, based on repeat analyses of the same sample for organic carbon, is +/- 2.5% of the measured TOC wt.% values. Details on the methods can be found in the supplementary material, File S1.

202

203 *3.5. Palaeoecological analysis*

204 Bulk samples were mechanically disaggregated in the laboratory to sub-centimetre size, with the
205 use of sharp chisels, and all recognisable macrofossils were counted and identified. The total dataset
206 comprises 1900 individuals of 141 species of bivalves, brachiopods and gastropods, which were
207 identified to the finest taxonomic level possible (Table S3). Shells that were originally calcitic are
208 preserved, whereas originally aragonitic shells occur as internal moulds. For bivalves and brachiopods,
209 the number of individuals was obtained by adding together the number of articulated specimens and the
210 highest number of right/left or dorsal/ventral valves. The number of gastropod individuals was equated
211 to the number of individual apices. Other taxonomic groups of benthic macro-invertebrates recorded in
212 the samples, including echinoderms and serpulids, were very rare and were not included in the dataset.

213 The number of species in each sample was used as a measure of richness (S). Evenness was
214 measured using the Simpson index of diversity (Simpson 1949), which is calculated as $1-\Sigma p_i^2$, where p is
215 the proportional abundance of species i. This index is an unbiased measure of evenness which ranges
216 from zero (one taxon dominates the assemblage completely) to one (all taxa have equal abundance;
217 Lande 1996).

218 Before multivariate elaboration, species occurring in only one sample were removed and samples
219 containing less than 12 individuals were excluded (mean sample size=35, min=12, max=86,
220 std.dev=18.2). Although 12 is a small sample size, the presence of multiple samples from each
221 sedimentary facies means that we are confident that the compositions of our fossil assemblages are
222 reliable (e.g., Bennington 2003). The resulting culled dataset comprises 52 samples with 78 species and
223 1663 individuals (87.5% of the original number of specimens). A two-way cluster analysis was
224 performed to describe groups of samples with similar faunal compositions (Q-mode). The clustering

algorithm used Bray–Curtis dissimilarity (Bray and Curtis 1957) and agglomerate nesting, coupled with Ward's method (Ward 1963), which adds samples to existing clusters that minimize the total sum of squares. Ward's method tends to produce dendrograms with well-defined clusters (Legendre and Legendre 1998). Biofacies were defined using Q-mode cluster analysis (cf., Ludvigsen et al. 1986). The cluster analysis was performed using the hclust() function in R's vegan package (R Core Team 2017). Data were ordinated using nonmetric multidimensional scaling (nMDS), a useful ordination method for detecting patterns of co-occurrence among taxa as well as ecological gradients (Legendre and Legendre 1998). Ordinations used Bray–Curtis dissimilarity, three axes, 100 restarts to prevent reaching a local optimum, and weighted averaging to calculate taxon scores. NMDS ordination was performed with the metaMDS() function in the vegan package of R (R Core Team 2017). This function rotates the nMDS solution via principal components analysis such that nMDS axis 1 (nMDS1) explains the principal source of variation of the data, and the other axes (nMDS2, nMDS3 and so on) explain decreasing percentages of the variation, as is characteristic of eigenvalue methods. NMDS ordination was performed (i) on the total dataset (ii) on samples from each separate locality; and (iii) on samples from each locality, analysing bivalves and brachiopods separately. Gastropods were too rare to analyse independently.

For each locality, correlations between the palaeoecological data (S, Evenness, nMDS1) and geochemical data from brachiopod shells ($\delta^{13}C$ and $\delta^{18}O$) and the bulk rock (TOC wt%) were made using the Spearman's rank correlation coefficient. Isotope data from brachiopod calcite were chosen instead of those of belemnites because their record is more complete throughout the two sections (e.g., no belemnites were found in the middle and upper part of the Sierra Palomera section), and because they are more likely to represent benthic environmental conditions. Possible temporal autocorrelations were tested for by applying the Durbin-Watson test (Durbin and Watson 1950), using the R package lmtest (R

248 Core Team 2017), and because some series returned positive results (Table S4), all data were
249 differentiated prior to estimating the Spearman's rank correlation coefficient (Kendall 1948).
250
251 **4. Results**
252
253 *4.1. Brachiopod and belemnite preservation*
254 Trace element analysis was undertaken on those samples of belemnites and brachiopods that
255 passed the initial CL-screening (Fig. 3), in order to provide additional screening of samples for possible
256 diagenetic alteration (Veizer 1983). Most of the investigated belemnites, with the exception of 5
257 samples, had Fe concentrations below 200 ppm and Mn concentrations below 100 ppm (Table S1, S2),
258 which are comparable with values recorded from other belemnites that are considered to be well-
259 preserved (e.g., Rosales et al. 2004; Alberti et al. 2012; Wierzbowski 2015). Recent brachiopod shells
260 (e.g., Morrison and Brand 1986; Brand et al. 2003) typically show low concentrations of Mn (4–450
261 ppm) and Fe (20–770 ppm). All the investigated brachiopods have elemental concentrations within these
262 limits (Table S1, S2), and their recorded values are comparable with other published Jurassic brachiopod
263 data (e.g., Price et al. 2013; Wierzbowski 2015). Thus, we consider that the brachiopods and belemnite
264 specimens analysed in this study were not significantly affected by diagenesis.
265
266 *4.2. Carbon and oxygen isotopes*
267 The cross-plot of $\delta^{18}O$ against $\delta^{13}C$ data shows very little correlation between micrite samples
268 from Sierra Palomera (Fig. 4). Most of $\delta^{18}O_{micrite}$ and $\delta^{13}C_{micrite}$ samples from Castrovido also have a
269 scattered pattern, except for a few points showing a linear trend towards negative values (up to -3‰
270 $\delta^{13}C$ and -7.8‰ $\delta^{18}O$), which are located at the base of the *Elegantulum* Subzone (Fig. 5). Although a

correlation between $\delta^{18}O$ and $\delta^{13}C$ values can occasionally be of primary origin (e.g., due to increased productivity linked to warmer temperatures), the covariance of $\delta^{18}O_{micrite}$ and $\delta^{13}C_{micrite}$ data from the *Elegantulum* Subzone Castrovido suggests that they might have been affected by diagenesis. Diagenetic recrystallization of carbonate takes place in the presence of water, and any carbonate precipitated is likely to have a $\delta^{18}O$ isotope value determined by pore-fluid composition and temperature (Immenhauser et al. 2002). Hence, a diagenetic overprint may have affected the *Elegantulum* Subzone $\delta^{18}O_{micrite}$ data from Castrovido. As pore-fluids have relatively low carbon content and the carbon reservoir in the rock is thought to be greater than that in the diagenetic fluid, bulk rock carbon isotope values are probably not significantly altered by diagenesis (Scholle and Arthur, 1980). The cross-plots of $\delta^{18}O$ and $\delta^{13}C$ values from the belemnites and brachiopods show no correlation between the data (Fig. 4), which demonstrates that the calcitic fossils have been affected by negligible diagenetic overprint (Marshall 1992).

The carbon and oxygen isotope data span from the Pliensbachian *Maragaritatus* Zone to the Toarcian *Bifrons* Zone (Figs. 5, 6; Table S1, S2). $\delta^{13}C_{micrite}$ values range between -2.8 and 2.9‰ at Castrovido and -0.3 and 2.7‰ at Sierra Palomera. At Sierra Palomera, $\delta^{13}C_{micrite}$ values record two marked negative excursions: one at the Pliensbachian/Toarcian boundary, and the other at the base of the *Elegantulum* Subzone (Fig. 6). At Castrovido, however, the Pliensbachian/Toarcian $\delta^{13}C_{micrite}$ negative excursion is less pronounced (Fig. 5). $\delta^{13}C_{bel}$ and $\delta^{13}C_{brach}$ values broadly replicate the micrite record, although gaps are present in the data. For example, belemnites were not found in the upper half of the Sierra Palomera section, where analysed brachiopods are also rare (Fig. 6). At both sections a gap is also present at the *Semicelatum-Elegantulum* transition, before and during the negative $\delta^{13}C_{micrite}$ excursion (Fig. 5, 6).

The $\delta^{18}O_{micrite}$ values range between -7.8‰ and -1.1‰ at Castrovido, and between -5.2‰ and -2.0‰ at Sierra Palomera. A well-defined vertical trend towards more negative values is recorded at

294 Sierra Palomera (Fig. 6). At Castrovido, this trend is less obvious and data are more scattered (Fig. 5).
295 As discussed above, the very negative $\delta^{18}O_{micrite}$ values at the base of the *Elegantulum* Subzone, might
296 be caused by diagenesis. Overall, $\delta^{18}O$ values of brachiopods are more positive than co-eval $\delta^{18}O_{micrite}$
297 values, but are less positive than the $\delta^{18}O$ values of co-eval belemnite samples (Figs. 5, 6). Both $\delta^{18}O_{bel}$
298 and $\delta^{18}O_{brac}$ values become more negative towards the upper part of the section, mirroring the pattern of
299 $\delta^{18}O_{micrite}$.
300
301 *4.3. Total organic carbon*
302 At Castrovido TOC values are very low (below 0.5 wt%) for most of the section, except from the
303 lower part of the *Elegantulum* Subzone, where they peak at 2.6 wt% (Fig. 5). At Sierra Palomera, the
304 TOC record shows high variability throughout the entire section, with peaks over 4 wt%, and one up to
305 5.92 wt% in the *Falciferum* Subzone (Fig. 6). Overall, the range of TOC values at Castrovido is
306 consistent with values measured at other early Toarcian Southern European sites of the Tethys (0.5–3
307 wt.%: Jenkyns 1988; Jenkyns et al. 2002; Hesselbo et al. 2007; Bodin et al. 2010), while at Sierra
308 Palomera they are exceeded in a few instances.
309
310 *4.4. Changes in the marine benthic communities*
311 4.4.1. Richness and diversity
312 The total dataset, which pools all samples from Castrovido and Sierra Palomera together, is
313 dominated by bivalves (69.5% of the species and 58.8% of the individuals), followed by brachiopods
314 (20.5% of species; 39.1% of individuals) and by the rarer gastropods (10% of species; 2.1% of
315 individuals). At Castrovido, evenness is mostly high overall (0.6-0.9), but drops to low values (0.2-0.5)
316 in the *Elegantulum* Subzone, where richness also has its lowest values (S=4; Fig. 5). The lowest values

of richness and evenness coincide with the highest values of TOC (up to 2.6 wt%) and more negative $\delta^{13}C_{micrite}$ values. In the Sierra Palomera section, evenness is generally high apart from during the *Elegantulum* and *Falciferum* subzones, where it drops to 0.1-0.3, with richness reaching peak values in the *Semicelatum* and *Falciferum* subzones (Fig. 6). At Sierra Palomera, changes in richness and evenness mirror lithological changes and TOC variations: lime mudstones, which overall have lower TOC values, are more diverse than marly intervals.

4.4.2. Biofacies change and faunal turnover

NMDS ordination shows that the two sections record similar patterns of faunal change (Fig. 7A-B). At both Castrovido and Sierra Palomera, samples from the lower part of the sections (*Spinatum* and *Tenuicostatum* zones) form distinct clusters, which do not overlap with samples from the upper part (*Bifrons* and *Serpentinum* subzones). This indicates that samples from the *Spinatum* and *Tenuicostatum* zones have a very different faunal composition compared to samples from the *Bifrons* and *Serpentinum* subzones. The same pattern is recorded when samples from the two sections are analysed together (total dataset, Fig. 7C), and when bivalves and brachiopods from each locality are analysed separately (Fig. S1).

Cluster analysis on the total dataset allowed the identification of groups of samples that contain a similar suite of taxa in similar proportions (i.e., ‘‘biofacies’’ *sensu* Ludvigsen 1986), and to identify their characteristic species (Figs. 7D, 8, Table 1). Biofacies B1, B2, and B3 are mainly represented by samples from the *Spinatum* and *Tenuicostatum* zones, with the exception of one sample from the *Serpentinum* Zone. Biofacies B1 is only recorded in samples from Sierra Palomera, and is dominated by epifaunally non-motile bivalves like *Gryphaea sublobata* (37%) and *Plicatula spinosa* (15%), while the rhynchonellid *Quadratirhynchia attenuata* (8%) is the most common brachiopod (Table 1). Biofacies

B2 is dominated by brachiopods, including the terebratulid *Lobothyris subpuncata* (34%), and the deep-infaunal species *Pleuromya alduini* (24%), while biofacies B3 is dominated by the pectinid *Pseudopecten aequivalvis* (24%, Table 1). Biofacies B4 includes samples from the *Elegantulum* Subzone only, and is dominated by the rhynchonellid *Soaresirhynchia bouchardi* (68%), followed by the pectinid *Parvamussium pumilum* (15%), the epifaunally attached *Plicatula auricula* (9%) and *Gryphaea crickleyensis* (4%). New brachiopod species appear after the *Elegantulum* Subzone, and are shared between Biofacies B5, B6 and B7. These biofacies contain a higher abundance and diversity of infaunal suspension feeding bivalves, compared to Biofacies B1 to B3. The pectinids *P. pumilum* (20%), *Entolium corneolum* (8%) and *Chlamys textoria* (7%) are the most abundant bivalves in B5, while amongst the brachiopods *Homoeorhynchia batalleri* (11%) and *Telothyris pirenaica* (10%) dominate (Table 1). Biofacies B6 is only recorded from Sierra Palomera and is dominated by the terebratulids *Telothyris jauberti* (17%) and *T. pirenaica* (12%). Biofacies B7 is also dominated by brachiopods, the most abundant being the terebratulid *Telothyris pirenaica* (24%) and the rhynchonellid *Homoeorhynchia meridionalis* (17%); among the bivalves, *P. pumilum* is still very common (10%). The carnivore *P. pumilum* is very common in post-extinction samples, together with rarer deposit-feeding bivalves of the families Nuculidae and Nuculanidae (Table 1), and grazing and omnivore gastropods (e.g., *Ampullospira?* and *Pleurotomaria* sp.; Table S3).

4.4.3. Correlation between ecological and environmental variables

Spearman's Rank correlations were performed between geochemical (TOC, $\delta^{13}C_{brach}$, $\delta^{18}O_{brac}$) and ecological (S, Evenness, nMDS1) data, for each locality. Ecological parameters were measured for the total dataset (S, Evenness, nMDS1), and for the bivalve (S_{biv}, $Evenness_{biv}$, $nMDS1_{biv}$) and brachiopod (S_{brach}, $Evenness_{brach}$, $nMDS1_{brach}$) datasets separately (Table 2). Correlations give

363 statistically significant results ($p<0.05$) in only a few instances out of the fifty-four possible
364 combinations (Table 2; Fig. S2). For the Castrovido samples, the only significant correlation we found is
365 that the bivalve community composition ($nMDS1_{biv}$) is negatively correlated with $\delta^{18}O_{brac}$ values. In
366 contrast, for the Sierra Palomera section, the richness and evenness of the entire fossil community (S,
367 Evenness) and of just the bivalves (S_{biv}, and $Evenness_{biv}$) are all negatively correlated with TOC. The
368 fact that the total dataset shows the same correlations as the bivalve-only dataset suggests that the
369 dominance of bivalves over brachiopods, in term of both richness and abundance, probably drives the
370 patterns of diversity and composition recorded in the entire community.
371
372 4.4.4. Extinction interval and sequence stratigraphic surfaces
373 In both sections, brachiopods go through a complete turnover in taxonomic composition at the
374 *Semicelatum/Elegantulum* boundary, while many bivalve species cross this interval (Figs. 9, 10). At
375 Castrovido, last occurrences of late Pliensbachian-early Toarcian brachiopods occur in the *Semicelatum*
376 Subzone, at the transgressive surface that separates cycles LJ3-2a and LJ3-2b. This surface is
377 characterised by an abrupt facies change from an interval dominated by lime mudstones to a thick
378 interval of marls, which suggest a change to a deeper depositional setting (Fig. 9). This surface is
379 followed by a ~ 2-m thick interval that is barren of macro-invertebrates, which corresponds to the
380 transgressive part of cycle LJ3-2b. *Soaresirhynchia bouchardi* is the only brachiopod, except one
381 occurrence of the inarticulate *Lingula* sp., to be present in the lower part of the *Elegantulum* Subzone,
382 together with the abundant pectinid *Parvamussium pumilum* and one specimen of the posidoniid *Bositra*
383 *?buchii*. They all occur in the regressive part of cycle LJ3-2b, and, specifically, the most abundant
384 species, *S. bouchardi*, first occurs at the maximum flooding surface. A suite of completely new

brachiopod species first occur at the top of the *Elegantulum* Subzone, in the lower, transgressive, part of cycle LJ3-3.

Unlike at Castrovido, last occurrences at Sierra Palomera cluster at the maximum flooding surface of cycle LJ3-2b, which occurs at the *Semicelatum-Elegantulum* transition (Fig. 10). The barren interval is thinner than at Castrovido (around 50 cm thick), and the following, regressive, part of cycle LJ3-2b, where new colonising species first occur, contains a more diverse benthic fauna than at Castrovido. The rhynchonellid brachiopod *S. bouchardi* dominates, and co-occurs with a diverse assemblage of bivalves: *P. pumilum*, *Pseudopecten aequivalvis*, *Pinna* sp., *Gryphaea* cf. *sublobata*, and *Nicaniella* sp.1. New early Toarcian brachiopod species appear at the top of the *Elegantulum* Subzone at Sierra Palomera, as at Castrovido, at the base of transgressive cycle LJ3-3.

5. Discussion

5.1. Correlation and interpretation of carbon-isotope excursions

Globally, the Pliensbachian/Toarcian boundary is characterized by a negative carbon-isotope excursion, which is recorded in marine bulk–rock carbonates, brachiopods, wood and organic matter (e.g., Hesselbo et al. 2007; Littler et al. 2010; Suan et al. 2010; Bodin et al. 2016; Ait-Itto et al. 2017). This negative excursion is most clearly recorded in our data at Sierra Palomera, where $\delta^{13}C_{micrite}$ data record a ~1.7‰ negative shift. The magnitude of this CIE is similar to the magnitudes of Pliensbachian/Toarcian boundary CIEs from other European sections; e.g., at Hawsker Bottoms, Yorkshire, England (Littler et al. 2010); in the Mochras Farm Borehole (Jenkyns and Clayton 1997); and at Peniche, Portugal (Hesselbo et al. 2007). At Peniche, for example, the negative CIE is ~2‰, which is comparable to the results of our study, whereas at other sections, such as in Morocco, an excursion of 3

to 4‰, spanning several 10s of metres, has been recorded (Bodin et al. 2016; Ait-Itto et al. 2017). A negative isotope excursion is not shown by belemnite and brachiopod samples, probably because of the patchiness of the data through the interval.

The second negative $\delta^{13}C_{micrite}$ excursion starts at the top of the *Semicelatum* Subzone, with the lowest values at the base of the *Elegantulum* Subzone, and equates to the negative CIE of the T-OAE (e.g., Hesselbo et al. 2007). At Sierra Palomera, TOC is already high prior to the proposed Toarcian CIE, and remains high after the event into the *Falciferum* Subzone. This differs from Castrovido and from other sites elsewhere in Europe, which record a TOC rise during the most negative part of the T-OAE (e.g., Hesselbo et al. 2000). These differences in the relative timing of organic matter enrichment and carbon isotope excursions illustrate the importance of local sedimentary processes and preservation, which appear largely independent from global forcing mechanisms (c.f., Trabucho-Alexandre et al. 2011). Acknowledging the global character of the CIE, and the non-synchronous distribution of organic rich-sediments in these sections and elsewhere (McArthur et al. 2008; Rodríguez-Tovar and Reolid 2013), as other authors have done previously (e.g. Bodin et al. 2016), we use the negative CIE to define the T-OAE. At both Castrovido and Sierra Palomera, the most negative part of the T-OAE $\delta^{13}C_{micrite}$ record corresponds to the interval of maximum flooding.

At Sierra Palomera, $\delta^{13}C_{micrite}$ values from the *Serpentinum* Zone (*Falciferum* Subzone) and *Bifrons* Zone are on average ~1‰ more positive than data derived from the same interval at Castrovido. This difference is most likely due to differences in the composition of the carbonate component of the rock samples at each site. For example, in modern settings, the $\delta^{13}C$ of neritic platform carbonates tends to be up to 4‰ more positive than pelagic carbonates produced by planktonic organisms such as coccoliths and foraminifera (Swart and Eberli 2005), and so it is expected that bulk rock carbonates from shallower settings would record more positive $\delta^{13}C_{micrite}$ values. The slightly more positive

$\delta^{13}C_{micrite}$ values recorded at Sierra Palomera, which was deposited in shallower water than Castrovido, are therefore consistent with such expectations. Carbon-isotopic enrichment of shallower water carbonates is thought to relate to a combination of factors including high levels of photosynthesis, which causes shallow waters to become enriched in the heavier isotope, and to the observation that aragonite tends to be enriched by approximately 1‰ compared to low Mg-calcite (Swart and Eberli 2005).

5.2. Estimated palaeotemperatures and early Toarcian warming

The oxygen-isotopic compositions of the belemnites and brachiopods, from both sites, record similar trends and become progressively more negative up section (Figs. 5, 6). Assuming a $\delta^{18}O_{seawater}$ value of -1, as typically inferred for a Jurassic world free of ice caps (Shackleton and Kennett 1975), and assuming that there were no major changes in the isotopic composition of seawater through the studied interval, our $\delta^{18}O_{brac}$ data indicate a rise in bottom water temperature from a mean of 20°C in the late *Margaritatus* to *Tenuicostatum* zones, to a peak of 25°C soon after the T-OAE extinction interval (Table 3, Table S1, S2). These estimated palaeotemperatures are consistent with data from other localities in the Iberian Peninsula where brachiopod calcite has been analysed, and the same assumptions applied, such as at Peniche in Portugal (Suan et al. 2008). In addition, warming across this interval is also indicated by $\delta^{18}O$ and Mg/Ca ratios of belemnite rostra from Portugal, England, Spain and Germany (Bailey et al. 2003; Rosales et al. 2004; van de Schootbrugge et al. 2005).

However, if the Jurassic $\delta^{18}O_{seawater}$ value at our study sites was closer to 0, then estimated palaeotemperatures would be ~5°C higher (Table 3), although the magnitude of the rise would be the same (cf., Kearsey et al., 2009). It has been suggested that there may have been transient development of icehouse conditions during the late Pliensbachian before the T-OAE (Price 1999, van de Schootbrugge et al. 2005; Suan et al 2010; Korte and Hesselbo 2011). If so, then the isotopic composition of Jurassic

454 seawater may have shifted from near 0 to -1 across the T-OAE, and the absolute temperature change
455 would have been less than 5°C (Table 3).

456 Apart from the potential for global changes in $\delta^{18}O_{seawater}$, shallow marine environments may be
457 affected by local or regional variations in evaporation, precipitation and runoff, and therefore the $\delta^{18}O_{brac}$
458 record could plausibly also reflect variations in both seawater temperature and salinity. Warming events
459 are likely to cause a reduction in surface seawater salinity due to changes to the hydrological cycle such
460 as higher continental runoff (e.g., Cohen et al. 2004). Given kinetic effects during evaporation and
461 precipitation, freshwater $\delta^{18}O$ is generally lower than that of marine water (Craig 1961). If post-
462 extinction brachiopods biomineralised in waters with elevated freshwater input, the $\delta^{18}O$ values of their
463 shells would therefore become more negative, leading to an overestimate of seawater temperature.
464 However, brachiopods are benthic animals, have preference for normal salinity seawaters (Brand et al.
465 2003), and both sites are below storm wave base in the Turmiel Formation (Comas-Rengifo et al. 1996).
466 Furthermore bottom seawaters are generally less affected by salinity changes than surface seawaters in
467 today's oceans (e.g., Lear et al. 2000). Therefore we consider that the recorded $\delta^{18}O_{brac}$ values were only
468 influenced to a minor extent, at most, by possible salinity changes.

469 Comparison between belemnite and brachiopod oxygen isotope compositions from the two
470 sections reveals that the $\delta^{18}O$ values of the belemnites are more positive (i.e., they biomineralised in
471 'cooler' waters) than the coeval brachiopods (Figs. 5, 6). This difference has been noted before on a
472 global-scale (Price et al. 2013), and in a range of local studies (e.g., Alberti et al. 2012; Mettam et al.
473 2014; Wierzbowski 2015). Although non-equilibrium processes may explain the oxygen isotopic
474 signatures of belemnite fossils (Immenhauser et al. 2016), the consistent difference between brachiopods
475 and belemnites is most simply explained by their different ecologies: belemnites were motile animals,
476 able to swim throughout the water column but which evidently biomineralised in deeper (cooler) waters

as modern coleoids do (Price et al. 2009). Brachiopods, being sessile, record the chemistry of the seawater at the site where they lived and are found, or from shallower (i.e., nearer sea-surface) settings if they have been transported downslope post-mortem. Thus, they are the preferred proxy group for Jurassic palaeotemperature studies (Price et al. 2013).

5.3. Faunal turnover and potential environmental drivers

At both localities, the pre-extinction faunal association of the *Tenuicostatum* Zone comprises Biofacies B3, in which the abundance of non-attached epifaunal suspension feeders (e.g., *Gryphaea* cf. *sublobata*; *Pseudopecten aequivalvis*) is indicative of relatively soft substrates and low energy conditions (Fürsich et. al 2001), while the presence of deep-infaunal bivalves like *Pleuromya* suggests well oxygenated bottom waters. This is consistent with what is observed in other localities of the Iberian Range, where the dominance of epifaunal suspension feeders and the scarcity of detritus and deposit feeders has been interpreted as indicative of a regime of low productivity, low turbidity, and low rate of sedimentation in moderately soft to firm substrates (e.g., Fürsich et. al 2001; Gahr 2005).

The first assemblage to colonize the soft bottom after the extinction event is dominated by small, opportunistic species, like the brachiopod *Soaresirynchia bouchardi*, and the epifaunal bivalves *Parvamussium pumilum* and *Plicatula auricula* (Biofacies B4, Figs. 9, 10). *S. bouchardi* has the distinctive features of an opportunistic organism (*sensu* Levinton 1970) as it shows basic external features (e.g., nearly smooth shells, sub-rounded outlines), morphological plasticity and simple internal architecture, and has a wide geographical distribution in the western Tethys (Gahr 2005; García Joral et al. 2011; Baeza-Carratalá et al. 2011). Smooth brachiopods were typical inhabitants of deep-sea environments in the Western Tethys (cf., Ager 1967; Vörös 1993, 2005). According to Vörös (2005), after the end-Permian extinction, deeper-water marine habitats operated as long-term reservoirs where

500 the evolutionary lineages of smooth morphotypes survived marine crises and from which, under
501 appropriate conditions, expanded to re-occupy shallow habitats. *S. bouchardi* was probably one of these
502 species adapted to deep-sea environments, which took advantage of the ecological void caused by the
503 early Toarcian extinction by colonizing shallower habitats (Baeza-Carratalá et al. 2017). The deepening
504 that occurred during the LJ3-2b cycle, might also have favoured this colonization.

505 Similarly, *P. pumilum* is considered a eurytopic opportunist able to adapt to a wide range of
506 environmental conditions, given its elevated abundance at certain levels in the Toarcian of the Tethys,
507 included laminated black shales (Johnson 1984). Furthermore, modern propeamussiids occupy an
508 entirely exceptional position with regard to feeding type among bivalves, as they have adapted to a
509 carnivorous life style, preying on copepods (Hicks and Marshall 1985), foraminifera, and different kinds
510 of eggs and larvae (Morton and Thurston 1989). Most extant species in the Propeamussiidae inhabit
511 bathyal or abyssal zones, and their carnivorous life style clearly represents an adaptation to such
512 environments in which suspended nutrients are usually scarce (Schneider et al. 2013).

513 The other post-extinction communities (i.e., Biofacies B5-B7) are somewhat similar in their
514 ecological characteristics to the pre-extinction ones but show a higher abundance and diversity of
515 infaunal suspension-feeding bivalves as well as common occurrences of the carnivorous epifaunal
516 bivalve *Parvamussium*. The most striking difference between pre- and post-extinction communities is in
517 taxonomic composition. At both sections, brachiopods go through a complete turnover through the
518 studied interval, whereas many bivalve species range through it, indicating that the Toarcian extinction
519 event had relatively little impact on this group, at least locally in the Iberian Ranges. García Joral et al.
520 (2011) interpreted this brachiopod turnover as being due to widespread extinctions brought about by the
521 rapid and pronounced increase in temperature at the *Tenuicostatum/Serpentinum* boundary. They
522 hypothesise that as temperatures rose, brachiopods were prevented from dispersing toward the northern,

cooler Arctic waters by the predominant southward currents along the Laurasian Seaway, and so were unable to escape the increasing seawater temperature (García Joral et al. 2011).

We found no significant correlation between $\delta^{18}O_{brac}$ and $nMDS1_{brac}$ in this study (Table 2), which suggests that temperature may not have been a major driver of brachiopod community composition, at least at these study sites, although this is not a direct test of the García Joral et al. (2011) hypothesis. In their multivariate analysis of Pliensbachian-Toarcian communities from the Cleveland Basin, UK, Danise et al. (2015) also found no evidence of correlation between $\delta^{18}O$ and benthic marine diversity, although in that case the oxygen-isotope data derived from belemnites not brachiopods. Intriguingly, although the significant negative correlation between $\delta^{18}O_{brac}$ and $nMDS1_{biv}$ suggests that seawater temperature possibly influenced the composition of bivalve communities, bivalves did not suffer intense extinction.

In contrast to the situation at Castrovido, the negative correlation between TOC and richness (S, S_{biv}) and evenness (Evenness, $Evenness_{biv}$) at Sierra Palomera (Table 2) suggests that changes in the total organic carbon content might have played a role in controlling benthic community diversity at the shallower site. The weight percent of organic carbon within sediments depends on different factors, such as palaeoproductivity, redox conditions and influx of terrigenous detrital material (Seiter et al. 2004), all of which could have affected faunal diversity. A palynological study conducted on the same section shows the disappearance of planktonic primary producers (e.g., acritarchs, dinoflagellates and *Tasmanites* prasinophyte algae) at the *Paltum-Semicelatum* Zone transition, and the dominance thereafter of terrestrially-derived palynomorphs throughout the rest of the section (Barrón et al. 1999). This suggests that low values of richness and evenness, especially in the upper part of the section, could have been caused by factors related to the loss of marine plankton and a high input of terrestrial organic matter. Terrestrial TOC input may have been episodic or highly seasonal and associated with episodes of

546 elevated freshwater influx to coastal environments, which would have resulted in temporary
547 stratification and local seafloor dysoxia. TOC values of up to 4 wt%, recorded in some horizons, are
548 close to McArthur et al.'s (2008) threshold of 5% TOC that typically characterises anoxic black shales.
549 The shallower setting of Sierra Palomera, and hence its relative proximity to the palaeocoastline
550 compared to Castrovido, might explain the higher input of terrigenous material, and the very different
551 trends in TOC between the two sites.
552
553 *5.4. Stratigraphic control on the timing of extinction*
554 The extinction horizon is expressed differently in the rock record at the two study sites, which
555 highlights the important role that stratigraphic processes play in determining the clustering of first and
556 last occurrences in sedimentary successions (Holland 1995, 2000). Stratigraphic condensation (e.g., at
557 flooding surfaces) can alter the apparent relative timing of first and last occurrences, making events
558 appear more closely spaced – less protracted in time – than they actually are (Holland 2000; 2015;
559 Nawrot et al. 2017). In this study, last occurrences occur at two flooding surfaces: a transgressive
560 surface at Castrovido, and a maximum flooding surface at Sierra Palomera (Figs. 9, 10). At Castrovido,
561 the more pronounced transgression at the *Semicelatum-Elegantulum* transition results in clustering of
562 last occurrence at the base of the LJ3-2b cycle and produces a thicker stratigraphic interval barren of
563 macrofauna (~2 metres thick). At Sierra Palomera, on the other hand, which records a more proximal
564 (onshore) depositional position than Castrovido, last occurrences peak at the stratigraphically higher
565 maximum flooding surface of cycle LJ3-2b, resulting in a much thinner interval barren of macrofauna
566 (~50 cm thick). The strong stratigraphic control on the distribution of species is readily demonstrated by
567 looking at the last occurrences of a few species in the two sections. *Lobothyris subpunctat*a, *L. arcta*,
568 and *Liospiriferina falloti* disappear at the transgressive surface at Castrovido, but have their last

occurrences at the maximum flooding surface in Sierra Palomera (Figs. 9, 10). The same species (i.e., with the same environmental tolerance), persisted longer at Sierra Palomera because of the shallower water depth compared to Castrovido. This further confirms the need to study multiple sections in the same sedimentary basin, along an onshore-offshore transect in order to better understand the timing and magnitude of an extinction event (Smith et al. 2001; Holland 2015; Danise and Holland 2017).

5.5. Timing of recovery, comparison with other localities and extinction events

Richness returns to pre-extinction values at the top of the *Elegantulum* Subzone at Sierra Palomera (Fig. 6), and at the base of the *Falciferum* Subzone at Castrovido (Fig. 5), indicating full recovery of benthic communities. Recovery is faster than at other Tethyan localities that are characterised by the development of anoxic/dysoxic conditions with the deposition of thick black shales. For instance, brachiopods did not recover in Northern Spain (Asturias and Basque–Cantabrian Basin) until the Middle Toarcian *Variabilis* Zone (García Joral and Goy 2009; García Joral et al. 2011). Similarly, in the Cleveland Basin, UK, black shale deposition was protracted until the lower part of the *Bifrons* Zone, and this noticeably delayed faunal recovery (Danise et al. 2013; 2015). In contrast, on the East Midland Shelf, UK, situated in a shallower, more hospitable setting compared to the Cleveland Basin, an increase in faunal diversity began earlier, within the upper *Exaratum* Subzone (Caswell and Coe 2012), which correlates with the *Elegantulum* Subzone of western Tethys. As noticed by García Joral et al. (2011), the recovery pattern recorded in early Toarcian sections resembles the pattern that occurred in the aftermath of the Late Permian mass extinction event, where recovery was more rapid in well oxygenated areas, but delayed in areas affected by anoxia (e.g., Twitchett et al. 2004; Foster et al. 2015). Hence, even if the development of anoxia was not the main, global cause of faunal loss across the early Toarcian, it plays an important role for faunal recovery in the immediate aftermath.

Results from our local study mirror those from a global analysis of early Jurassic marine organisms, which found that the early Toarcian event selected against sessile suspension feeders (Dunhill et al. 2018a). Similar results have been found for other Mesozoic warming-related extinction events, such as the Late Permian (e.g., Rhodes and Thayer 1991, Erwin et al. 2002) and the Late Triassic mass extinctions (Dunhill et al. 2018a, 2018b). In particular, the global scale impact of the early Toarcian event was extraordinarily important for the articulate brachiopods: two major orders, Spiriferinida and Athyridida, and about 67% of the genera belonging to the order Rhynchonellida disappeared (Vörös 2002; Vörös et al. 2016; Manceñido 2000). The decline of brachiopods, which had already started with the Late Permian and Late Triassic mass extinctions, represent a fundamental change in the taxonomic structure and ecological architecture of marine ecosystems, and contributed to the shift to the molluscan Modern Fauna (Sepkoski 1981;1996; Bambach et al. 2002).

6. Conclusions

Our geochemical, palaeontological and stratigraphic study of two study sites in the Iberian Range, Spain, that originally lay along an onshore-offshore transect, has increased our understanding of the early Toarcian extinction event in the western Tethys. High-resolution analyses of $\delta^{13}C$, $\delta^{18}O$ and TOC from bulk rock samples, coupled with $\delta^{13}C$ and $\delta^{18}O$ analyses of belemnites and brachiopods, has enabled us to characterise the geochemical signatures of the Pliensbachian/Toarcian boundary and the early Toacian (T-OAE) events in the Iberian Range. A negative CIE at the Pliensbachian/Toarcian boundary is recorded at both sections, but is more pronounced at Sierra Palomera than at Castrovido. A negative CIE in the lower part of the *Elegantulum* subzone is recorded at both sections, and coincides with organic enrichment at Castrovido but not at Sierra Palomera. The apparent timing of the early Toarcian extinction of the benthic fauna also differs between study sites, indicating the importance of

615 understanding local stratigraphy when interpreting the fossil record. Last-occurrences cluster at a
616 transgressive surface at the deeper water site of Castrovido but at the maximum flooding surface at the
617 shallower site of Sierra Palomera.

618 The early Toarcian extinction event caused a complete turnover in the brachiopod community
619 locally, but most bivalve species survived. Spearman's rank correlations between geochemical and
620 ecological variables demonstrate a strong correlation between changes in TOC, bivalve richness and
621 evenness at Sierra Palomera. We hypothesis that high organic content from episodic continental runoff
622 locally inhibited species diversity at the shallower study site, possibly due to associated changes such as
623 local dysoxia and salinity stratification. At Castrovido, a significant correlation between the $\delta^{18}O$ record
624 of brachiopod calcite and the ecological metric nMDS1 suggests that rising seawater temperature may
625 have affected the composition of bivalve communities at the deeper water site.

626 Our study has uncovered a number of key differences in the stratigraphic, geochemical and
627 palaeoecological records of the two study sites, and in the responses of the different taxonomic groups to
628 the early Toarcian extinction event. This shows the value of analysing multiple sections along a depth
629 transect rather than extrapolating from a single study site, and of integrating fossil and geochemical data
630 from the same samples. Analysing different taxonomic groups from multiple sites through the same
631 event is likely to provide greater insights into understanding the responses of marine communities to
632 past climate change and environmental perturbation.

633

634 **Acknowledgements**

635 This project was supported by Natural Environment Research Council (NERC) grant to R.J.
636 Twitchett (NE/I005641/1), and by project CGL201566604-R of the Spanish Ministerio de Economía y
637 Competitividad to J.J. Gómez. We thank F. García Joral for showing his collection of Early Jurassic

brachiopods for comparison; Silvia Menéndez and Graciela Delvene for access to the bivalve collection of the Museo Geominero, Madrid; Jodie Fisher and Chiara Consolaro for TOC analyses; University of Copenhagen for trace element analysis.

References

Aberhan, M., 2001. Bivalve palaeobiogeography and the Hispanic Corridor: time of opening and effectiveness of a proto-Atlantic seaway. Palaeogeogr. Palaeoclimatol. Palaeoecol. 165, 375–394.

Ager, D.V., 1967. Some Mesozoic brachiopods in the Tethys region. In: Adams, C.G., Ager, D.V. (Eds.), Aspects of Tethyan Biogeography. 7. Systematics Association Publication, pp. 135–151.

Ait-Itto, F-Z., Price, G.D., Addi, A.A., Chafiki, D., Mannani, I., 2017. Bulk-carbonate and belemnite carbon-isotope records across the Pliensbachian-Toarcian boundary on the northern margin of Gondwana (Issouka, Middle Atlas, Morocco). Palaeogeogr. Palaeoclimatol. Palaeoecol. 466, 128–136.

Alberti, M., Fürsich, F.T., Pandey, D.K., Ramkumar, M., 2012. Stable isotope analyses of belemnites from the Kachchh Basin, western India: paleoclimatic implications for the Middle to Late Jurassic transition. Facies 58, 261–278.

Anderson, T.F., Arthur, M.A., 1983. Stable isotopes of oxygen and carbon and their application to sedimentological and paleoenvironmental problems. In: Arthur, M.A., Anderson, T.F., Kaplan, I.R., Veizer, J., Land, L. (Eds.), Stable isotopes in sedimentary geology: SEPM Short Course, 10, pp. 1–151.

Arias, C., 2013. The early Toarcian (early Jurassic) ostracod extinction events in the Iberian Range: The effect of temperature changes and prolonged exposure to low dissolved oxygen concentrations. Palaeogeogr. Palaeoclimatol. Palaeoecol. 387, 40–55.

661 Aurell, M., Robles, S., Bádenas, B., Rosales, I., Quesada, S., Meléndez, G., Garcıa-Ramos, J.C., 2003.
662 Transgressive–regressive cycles and Jurassic palaeogeography of northeast Iberia. Sediment. Geol.
663 162, 239–271.
664 Baeza-Carratalá, J.F., García Joral, F., Tent-Manclús, J.E., 2011. Biostratigraphy and
665 palaeobiogeographic affinities of the Jurassic brachiopod assemblages from Sierra Espuña
666 (Maláguide Complex, Internal Betic Zones, Spain). J. Iber. Geol. 37, 137–151.
667 Baeza-Carratalá, J.F., García Joral, F., Giannetti, A., Tent-Manclús, J.E., 2017. Evolution of the last
668 koninckinids (Athyridida, Koninckinidae), a precursor signal of the early Toarcian mass extinction
669 event in the Western Tethys. Palaeogeogr. Palaeoclimatol. Palaeoecol. 429, 41–56.
670 Bailey, T.R., Rosenthal, Y., McArthur, J.M., Van De Schootbrugge, B., Thirlwall, M.F., 2003.
671 Paleoceanographic changes of the Late Pliensbachian–Early Toarcian interval: a possible link to
672 the genesis of an Oceanic Anoxic Event. Earth Planet. Sci. Lett. 212, 307–320.
673 Bambach, R.K., Knoll, A.H., Sepkoski, J.J., 2002, Anatomical and ecological constraints on
674 Phanerozoic animal diversity in the marine realm, PNAS 99, 6854–6859.
675 Barbin, V., 2013. Application of cathodoluminescence microscopy to recent and past biological
676 materials: a decade of progress. Miner. Petrol. 107, 353–362.
677 Barrón, E., Comas-Rengifo, M.J., Trincão, P., 1999. Estudio palinológico del tránsito
678 Pliensbachiense/Toarciense en la Rambla del Salto (Sierra Palomera, Teruel, España). Cuadernos
679 de Geología Ibérica 25, 181–187.
680 Belanger, C.L., 2012. Individual to community-level faunal responses to environmental change from a
681 marine fossil record of Early Miocene global warming. PLoS ONE 7(4), e36290.
682 Bennington, J.B., 2003. Transcending patchiness in the comparative analysis of paleocommunities: a
683 test case from the Upper Cretaceous of New Jersey. Palaios 18, 22–33.

684 Bjerrum, C.J., Surlyk, F., Callomon, J.H., Slingerland, R.L., 2001. Numerical paleoceanographic study
685 of the Early Jurassic Transcontinental Laurasian Seaway. Paleoceanography 16, 390–404.
686 Bodin, S., Mattioli, E., Frölich, S., Marshall, J.D., Boutib, L., Lahsini, S., Redfern, J., 2010. Toarcian
687 carbon isotope shifts and nutrient changes from the Northern margin of Gondwana (High Atlas,
688 Morocco, Jurassic): palaeoenvironmental implications. Palaeogeogr. Palaeoclimatol. Palaeoecol.
689 297, 377–390.
690 Bodin, S., Krencker, F., Kothe, T., Hoffmann, R., Mattioli, E., Heimhofer, U., Kabiri, L., 2016.
691 Perturbation of the carbon cycle during the late Pliensbachian – Early Toarcian: New insight from
692 high–resolution carbon isotope records in Morocco. J. Afr. Earth Sci. 116, 89–104.
693 Brand, U., Logan, A., Hiller, N., Richardson, J., 2003. Geochemistry of modern brachiopods:
694 Application and implications for oceanography and paleoceanography. Chem. Geol. 198, 305–
695 334.
696 Bray, J.R., Curtis, J.T., 1957. An ordination of upland forest communities of southern Wisconsin. Ecol.
697 Monog. 27, 325–349.
698 Brazier, J.-M., Suan, G., Tacail, T., Simon, L., Martin, J.E., Mattioli, E., Balter, V., 2015. Calcium
699 isotope evidence for dramatic increase of continental weathering during the Toarcian oceanic
700 anoxic event (Early Jurassic). Earth Planet. Sci. Lett. 411, 164–176.
701 Burgess, S.D., Bowring, S.A., Fleming, T.H., Elliot, D.H., 2015. High-precision geochronology links
702 the Ferrar large igneous province with early-Jurassic ocean anoxia and biotic crisis. Earth Planet.
703 Sci. Lett. 415, 90–99.
704 Callomon, J.H., 1979. Marine boreal Bathonian fossils from the northern North Sea and their
705 palaeogeographical significance. Proc. Geol. Assoc. Lond. 90, 163–169.

706 Caruthers, A.H., Smith, P.L., Gröcke, D.R., 2013. The Pliensbachian–Toarcian (Early Jurassic)
707 extinction, a global multi-phased event. Palaeogeogr. Palaeoclimatol. Palaeoecol. 386, 104–118.
708 Caswell, B.A., Coe, A.L., 2012. A high-resolution shallow marine record of the Toarcian (Early
709 Jurassic) Oceanic Anoxic Event from the East Midlands Shelf, UK. Palaeogeogr. Palaeoclimatol.
710 Palaeoecol. 365–366, 124–135.
711 Caswell, B.A., Coe, A.L., Cohen, A.S., 2009. New range data for marine invertebrate species across the
712 early Toarcian (Early Jurassic) mass extinction. J. Geol. Soc. London 166, 859–872.
713 Cecca, F., Macchioni, F., 2004. The two Early Toarcian (Early Jurassic) extinction events in
714 ammonoids. Lethaia 37, 35–56.
715 Cohen, A.S., Coe, A.L., Harding, S.M., Schwark, L., 2004. Osmium isotope evidence f or the regulation
716 of atmospheric CO_2 by continental weathering. Geology 32, 157–160.
717 Comas-Rengifo, M.J., 1985. El Pliensbachiense de la Cordillera Ibérica. Colección Tesis Doctorales,
718 1985. Univ. Complutense Madrid, Spain. 594 pp.
719 Comas-Rengifo, M.J., Goy, A., Yébenes, A., 1988. El Lias en el Sector Sur occidental de la Sierra de la
720 Demanda (Castrovido, Burgos). Cienc. Tierra Geol. 11, 119–141.
721 Comas-Rengifo, M.J., Gómez, J.J., Goy, A., Arias, C.F., Bernad, J., García Joral, F., Herrero, C.,
722 Martínez, G., Perilli, N., 1996. The Toarcian in the Rambla del Salto (Sierra Palomera) section. 1st
723 Toarcian and 4th Aalenian working groups meeting. International subcomission on Jurassic
724 stratigraphy. Field Trip Iberian Range Guide Book, pp. 27– 48.
725 Craig, H., 1961. Isotopic variations in meteoric waters. Science 133, 1702–1703.
726 Damborenea, S.E., 2002. Jurassic evolution of Southern Hemisphere marine palaeobiogeographic units
727 based on benthonic bivalves. Geobios 35, 51–71.

728 Danise, S., Holland, S.M., 2017. Faunal response to sea-level and climate change in a short-lived
729 seaway: Jurassic of the Western Interior, U.S.A. Palaeontology 60, 213–232.
730 Danise, S., Twitchett, R.J., Little, C.T.S., Clémence, M.-E., 2013. The impact of global warming and
731 anoxia on marine benthic community dynamics: An example from the Toarcian (Early Jurassic).
732 PLoS ONE 8, e56255.
733 Danise, S., Twitchett, R.J., Little, C.T.S., 2015. Environmental controls on Jurassic marine ecosystems
734 during global warming. Geology 43, 263–266.
735 Dera, G., Neige, P., Dommergues, J., Brayard, A., 2011. Ammonite paleobiogeography during the
736 Pliensbachian–Toarcian crisis (Early Jurassic) reflecting paleoclimate, eustasy, and extinctions.
737 Glob. Planet. Change 78, 92–105.
738 Dunhill, A.M., Foster, W.J., Azaele, S., Sciberras, J., Twitchett, R.J., 2018a. Modelling determinants of
739 extinction across two Mesozoic hyperthermal events. Proc. R. Soc. Lond. B 285, 20180404.
740 Dunhill, A.M., Foster, W.J., Sciberras, J., Twitchett, R.J., 2018b. Impact of the Late Triassic Mass
741 Extinction on functional diversity and composition of marine ecosystems. Palaeontology 61, 133–
742 148
743 Durbin, J., Watson, G.S., 1950. Testing for serial correlation in least squares regression I. Biometrika
744 37, 409–428.
745 Erwin, D.H., Bowring, S.A., Yugan, J., 2002. End-Permian mass extinctions: a review. Geol. Soc. 356,
746 363–384.
747 Foster, W.J., Danise, S., Sedlacek, A., Price, G.D., Hips, K., Twitchett, R.J., 2015. Environmental
748 controls on the post-Permian recovery of benthic, tropical marine ecosystems in western
749 Palaeotethys (Aggtelek Karst, Hungary). Palaeogeogr. Palaeoclimatol. Palaeoecol. 440, 374–394.

Fürsich, F.T., Berndt, R., Scheuer, T., Gahr, M.E., 2001. Comparative ecological analysis of Toarcian (Lower Jurassic) benthic faunas from southern France and east-central Spain. Lethaia 34, 169–199.

Gahr, M., 2002. Palökologie des Makrobenthos aus dem Unter-Toarc SW-Europas. Beringeria 31, 3–204.

Gahr, M., 2005. Response of Lower Toarcian (Lower Jurassic) macrobenthos of the Iberian Peninsula to sea level changes and mass extinction. J. Iberian Geol. 31, 197–215.

García Joral, F., Goy, A., 2009. Toarcian (Lower Jurassic) brachiopods in Asturias (Northern Spain): stratigraphic distribution, critical events and palaeobiogeography. Geobios 42, 255–264.

García Joral, F., Gómez, J.J., Goy, A., 2011. Mass extinction and recovery of the Early Toarcian (Early Jurassic) brachiopods linked to climate change in northern and central Spain. Palaeogeogr. Palaeoclimatol. Palaeoecol. 302, 367–380.

Gómez, J.J., Goy A., 2005. Late Triassic and Early Jurassic palaeogeographic evolution and depositional cycles of the Western Tethys Iberian platform system (Eastern Spain). Palaeogeogr. Palaeoclimatol. Palaeoecol. 222, 77–94.

Gómez, J.J., Fernández-López, S.R., 2006. The Iberian Middle Jurassic carbonate-platform system: Synthesis of the palaeogeographic elements of its eastern margin (Spain). Palaeogeogr. Palaeoclimatol. Palaeoecol. 236, 190–205.

Gómez, J.J., Arias, C., 2010. Rapid warming and ostracods mass extinction at the Lower Toarcian (Jurassic) of central Spain. Mar. Micropaleontol. 74, 119–135.

Gómez, J.J., Goy, A., 2011. Warming-driven mass extinction in the Early Toarcian (Early Jurassic) of northern and central Spain. Correlation with other time-equivalent European sections. Palaeogeogr. Palaeoclimatol. Palaeoecol. 306, 176–195.

773 Gómez, J.J., Comas-Rengifo, M.J., Goy, A., 2003. Las unidades litoestratigráficas del Jurásico inferior
774 de las cordilleras Ibérica y Costero Catalana. Rev. Soc. Geol. Esp. 16, 227–237.
775 Gómez, J.J., Goy, A., Canales, M.L., 2008. Seawater temperature and carbon isotope variations in
776 belemnites linked to mass extinction during the Toarcian (Early Jurassic) in Central and Northern
777 Spain. Comparison with other European sections. Palaeogeogr. Palaeoclimatol. Palaeoecol. 258,
778 28–58.
779 Hesselbo, S.P., Gröcke, D.R., Jenkyns, H.C., Bjerrun, C.J., Farrimond, P., Morgans Bell, H.S., Green,
780 O.R., 2000. Massive dissociation of gas hydrate during a Jurassic oceanic anoxic event. Nature
781 406, 392–395.
782 Hesselbo, S.P., Jenkyns, H.C., Duarte, L.V., Oliveira, L.C.V., 2007. Carbon–isotope record of the Early
783 Jurassic (Toarcian) Oceanic Anoxic Event from fossil wood and marine carbonate (Lusitanian
784 Basin, Portugal). Earth Planet. Sci. Lett. 253, 455–470.
785 Hicks, G.R.F., Marshall B.A., 1985. Sex selective predation of deepsea meiobenthic copepods by
786 pectinacean bivalves and its influence on copepod sex ratios. New Zeal. J. Mar. Fresh. 19, 227–
787 231.
788 Holland, S.M., 1995. The stratigraphic distribution of fossils. Paleobiology 21, 92–109.
789 Holland, S.M., 2000. The quality of the stratigraphic record – a sequence stratigraphic perspective. In:
790 Erwin, D.H., Wing, S.L. (Eds), Deep time: paleobiology's perspective. The Paleontological
791 Society, Lawrence, KS., pp. 148–168.
792 Holland, S.M., 2015. The stratigraphy of mass extinction. Palaeontology 58, 903–924.
793 Kearsey, T., Twitchett, R.J., Price, G.D., Grimes, S.T., 2009. Isotope excursions and palaeotemperature
794 estimates from the Permian/Triassic boundary in the Southern Alps (Italy). Palaeogeogr.,
795 Palaeoclimatol., Palaeoecol. 279, 29–40.

796 Korte, C., Hesselbo, S.P., 2011. Shallow marine carbon and oxygen isotope and elemental records
797 indicate icehouse-greenhouse cycles during the Early Jurassic. Paleoceanography 26, PA4219.
798 Imai, N., Terashima, S., Itoh, S., Ando, A., 1996. Compilation of analytical data on nine GSJ
799 geochemical reference samples, "Sedimentary Rock Series". Geostand. Newslett. 20, 165–216.
800 Immenhauser, A., Kenter, J.A., Ganssen, G., Bahamonde, J.R., Van Vliet, A., Saher, M.H., 2002. Origin
801 and significance of isotope shifts in Pennsylvanian carbonates (Asturias, NW Spain). J. Sediment.
802 Res. 72, 82–94.
803 Immenhauser, A., Schöne, B. R., Hoffmann, R., Niedermayr, A., 2016. Mollusc and brachiopod skeletal
804 hard parts: Intricate archives of their marine environment. Sedimentology 63, 1–59.
805 Izumi, K., Miyaji, T., Tanabe, K., 2012. Early Toarcian (Early Jurassic) oceanic anoxic event recorded
806 in the shelf deposits in the northwestern Panthalassa: evidence from the Nishinakayama formation
807 in the Toyora area, west Japan. Palaeogeogr. Palaeoclimatol. Palaeoecol. 315–316, 100–108.
808 Jenkyns, H.C., 1988. The early Toarcian (Jurassic) anoxic event; stratigraphic, sedimentary and
809 geochemical evidence. Am. J. Sci. 288, 101–151.
810 Jenkyns, H.C., 2010. Geochemistry of oceanic anoxic events. Geochem., Geophys., Geosy. 11, Q03004.
811 Jenkyns, H.C., Clayton, C.J., 1997. Lower Jurassic epicontinental carbonates and mudstones from
812 England and Wales: chemostratigraphic signals and the early Toarcian anoxic event.
813 Sedimentology 44, 687–706.
814 Jenkyns, H.C., Gröcke, D.R., Hesselbo, S.P., 2001. Nitrogen isotope evidence for water mass
815 denitrification during the Early Toarcian (Jurassic) oceanic anoxic event. Paleoceanography 16,
816 593–603.

817 Jenkyns, H.C., Jones, C.E., Gröcke, D.R., Hesselbo, S.P., Parkinson, D.N., 2002. Chemostratigraphy of
818 the Jurassic system: applications, limitations and implications for palaeoceanography. J. Geol.
819 Soc. London 159, 351–378.
820 Johnson, A.L.A., 1984. The palaeobiology of the bivalve families Pectinidae and Propeamussiidae in the
821 Jurassic of Europe. Zitteliana 11, 1–235.
822 Kemp, D.B., Coe, A.L., Cohen, A.S., Schwark, L., 2005. Astronomical pacing of methane release in the
823 Early Jurassic period. Nature 437, 396–399.
824 Kendall, M.G., 1948. Rank correlation methods. Oxford, England, Griffin, 160 pp.
825 Lande, R., 1996. Statistics and partitioning of species diversity, and similarity among multiple
826 communities. Oikos 76, 5–13.
827 Lear, C.H., Elderfield, H., Wilson, P. A., 2000. Cenozoic deep-sea temperatures and global ice volumes
828 from Mg/Ca in benthic foraminiferal calcite. Science 287, 269–272.
829 Legendre, P., Legendre, L., 1998. Numerical Ecology, 2nd edn. Elsevier, 853 pp.
830 Levinton, J.S., 1970. The paleoecological significance of opportunistic species. Lethaia 3, 69–78.
831 Little, C.T.S., Benton, M.J., 1995. Early Jurassic mass extinction: a global long-term event. Geology 23,
832 495–498.
833 Littler, K., Hesselbo, S.P., Jenkyns, H.C., 2010. A carbon–isotope perturbation at the Pliensbachian–
834 Toarcian boundary: evidence from the Lias Group, NE England. Geol. Mag. 147,181–192.
835 Ludvigsen, R., Westrop, S.R., Pratt, B.R., Tuffnell, P.A., Young, G.A., 1986. Dual biostratigraphy:
836 Zones and biofacies. Geosci. Can. 13, 139–154.
837 Manceñido, M.O., 2002. Paleobiogeography of Mesozoic brachiopod faunas from Andean–Patagonian
838 areas in a global context. Geobios 35, 176–192.

839 Marshall, J.D., 1992. Climatic and oceanographic isotopic signals from the carbonate rock record and
840 their interpretation. Geol. Mag. 129, 134–160.
841 Martindale R.C., Aberhan, M., 2017. Response of macrobenthic communities to the Toarcian Oceanic
842 Anoxic Event in northeastern Panthalassa (Ya Ha Tinda, Alberta, Canada). Palaeogeogr.
843 Palaeoclimatol. Palaeoecol. 478, 103–112.
844 McArthur, J.M., Donovan, D.T., Thirlwall, M.F., Fouke, B.W., Mattey, D., 2000. Strontium isotope
845 profile of the early Toarcian (Jurassic) oceanic anoxic event, the duration of ammonite biozones,
846 and belemnite palaeotemperatures. Earth Plan. Sci. Lett. 179, 269–285.
847 McArthur, J.M., Algeo, T.J., van de Schootbrugge, B., Li, Q., Howarth, R.J., 2008. Basinal restriction,
848 black shales, Re-Os dating, and the Early Toarcian (Jurassic) oceanic anoxic event.
849 Paleoceanography 23, PA4217.
850 Mettam, C., Johnson, A.L.A., Nunn, E.V., Schöne, B.R., 2014. Stable isotope ($\delta^{18}O$ and $\delta^{13}C$)
851 sclerochronology of Callovian (Middle Jurassic) bivalves (*Gryphaea (Bilobissa) dilobotes*) and
852 belemnites (*Cylindroteuthis puzosiana*) from the Peterborough Member of the Oxford Clay
853 Formation (Cambridgeshire, England): Evidence of palaeoclimate, water depth and belemnite
854 behaviour. Palaeogeogr. Palaeoclimatol. Palaeoecol. 399, 187–201.
855 Morrison, J.O., Brand, U., 1986. Geochemistry of recent marine invertebrates. Geosci. Can. 13, 237–
856 254.
857 Morton, B., Thurston, M.H., 1989. The functional morphology of *Propeamussium lucidum* (Bivalvia:
858 Pectinacea), a deepsea predatory scallop. J. Zool. 218, 471–496.
859 Nawrot, R., Scarponi, D., Azzarone, M., Dexter, T.A., Kusnerik, K.M., Wittmer, J.M., Amorosi, A.,
860 Kowalewski, M., 2018. Stratigraphic signatures of mass extinctions: ecological and sedimentary
861 determinants Proc. R. Soc. B, 20181191.

Nieuwenhuize, J., Maas, Y.E.M, Middelburg, J.J., 1994. Rapid analysis of organic carbon and nitrogen in particulate materials. Mar. Chem. 45, 217–224.

Osete, M.L., Gialanella, P.R., Gómez, J.J., Villalaín, J.J., Goy, A., Heller, F., 2007. Magnetostratigraphy of Early–Middle Toarcian expanded sections from the Iberian Range (central Spain). Earth Planet. Sci. Lett. 259, 319–332.

Parkinson D., Curry G.B., Cusack M., Fallick A.E., 2005. Shell structure, patterns and trends of oxygen and carbon stable isotopes in modern brachiopod shells. Chem. Geol. 219, 193–235.

Price, G.D., 1999. The evidence and implications of polar ice during the Mesozoic, Earth Sci. Rev., 48, 183–210.

Price, G.D., Twitchett, R.J., Smale, C. Marks, V., 2009. Isotopic analysis of the life history of the enigmatic squid *Spirula spirula*, with implications for studies of fossil cephalopods. Palaios 24, 273–279.

Price, G.D., Twitchett, R.J., Wheeley, J.R., Buono, G., 2013. Isotopic evidence for long term warmth in the Mesozoic. Sci. Rep. 3, 1438.

Quesada S., Robles S., Rosales I., 2005. Depositional architecture and transgressive–regressive cycles within Liassic backstepping carbonate ramps in the Basque–Cantabrian basin, northern Spain. J. Geol. Soc. 162, 531–548.

R Core Team, 2017. R: a language and environment for statistical computing, v. 3.3.3. http://www.R-project.org/.

Rhodes, M.C., Thayer, C.W., 1991. Mass extinctions: ecological selectivity and primary production. Geology 19, 877–880.

883 Rodríguez-Tovar, F.J., Reolid, M., 2013. Environmental conditions during the Toarcian Oceanic Anoxic
884 Event (T-OAE) in the westernmost Tethys: influence of the regional context on a global
885 phenomenon. Bull. Geosci. 88, 697–712.
886 Rosales, I., Quesada, S., Robles, S., 2001. Primary and diagenetic isotopic signals in fossils and
887 hemipelagic carbonates: the Lower Jurassic of northern Spain. Sedimentology 48, 1149–1169.
888 Rosales, I., Quesada, S., Robles, S., 2004. Paleotemperature variations of Early Jurassic seawater
889 recorded in geochemical trends of belemnites from the Basque–Cantabrian basin, northern Spain,
890 Palaeogeogr. Palaeocl., 203, 253–275.
891 Salas, R., Guimerá, J., Mas, R., Martín-Closas, C., Meléndez, A., Alonso, A., 2001. Evolution of the
892 Mesozoic Central Iberian Rift System and its Cainozoic inversion (Iberian Chain). In: Ziegler,
893 P.A., Cavazza, W., Robertson, A.H.F., Crasquin-Soleau, S. (Eds.), Peri-Tethys Memoir 6: Peri-
894 Tethyan Rift/Wrench Basins and Passive Margins. Mém. Mus. Natn. Hist. Nat. 186, Paris, France,
895 pp. 145–185.
896 Schneider, S., Crampton, J.S., Lukeneder, A., 2013. Propeamussiidae, Inoceramidae, and other Bivalvia
897 from the Lower Cretaceous Puez Formation (Valanginian–Cenomanian; Dolomites, South Tyrol,
898 Italy). Cretac. Res. 46, 216–231.
899 Scholle, P.A., Arthur, M.A., 1980. Carbon isotope fluctuations in Cretaceous pelagic limestones:
900 potential stratigraphic and petroleum exploration tool. AAPG Bulletin 64, 67–87.
901 Seiter, K., Hensen, C., Schröter, J., Zabel, M., 2004. Organic carbon content in surface sediments—
902 defining regional provinces. Deep Sea Res. Part I: Oceanogr. Res. Pap. 51, 2001–2026.
903 Sepkoski, J.J., 1981. A factor analytic description of the Phanerozoic marine fossil record. Paleobiology
904 7, 36 – 53.

905 Sepkoski, J.J., 1996. Competition in macroevolution: the double wedge revisited. In, Jablonski, D.,
906 Erwin, D.H., Lipps, J.H. (Eds.), Evolutionary Paleobiology, University of Chicago Press, Chicago,
907 pp. 211–255.
908 Shackleton, N.J., Kennett, J.P., 1975. Paleotemperature history of the Cenozoic and the initiation of
909 Antarctic glaciation: oxygen and carbon isotope analyses in DSDP sites 277, 279, and 289. Initial
910 Reports of the Deep Sea 29, 743–755.
911 Simpson, E.H., 1949, Measurement of diversity. Nature 163, 688.
912 Smith, A.B., Gal E., Monk, S.N., 2001. Sea-level change and rock-record bias in the Cretaceous: a
913 problem for extinction and biodiversity studies. Paleobiology 27, 241–253.
914 Suan, G., Mattioli, E., Pittet, B., Mailliot, S., Lécuyer, C., 2008. Evidence for major environmental
915 perturbation prior to and during the Toarcian (Early Jurassic) oceanic anoxic event from the
916 Lusitanian Basin, Portugal. Paleoceanography 23, PA1202.
917 Suan, G., Mattioli, E., Pittet, B., Lécuyer, C., Suchéras–Marx, B., Duarte, L.V., Philippe, M., Reggiani,
918 L., Martineau, F., 2010. Secular environmental precursors to Early Toarcian (Jurassic) extreme
919 climate changes. Earth Planet. Sci. Lett. 290, 448–458.
920 Swart, P.K., Eberli, G.P., 2005. The nature of the $\delta^{13}C$ of periplatform sediments: Implications for
921 stratigraphy and the global carbon cycle. Sediment. Geol. 175, 115–129.
922 Trabucho-Alexandre, J., van Gilst, R.I., Rodrıguez-Lopez, J.P., de Boer, P.L., 2011. The sedimentary
923 expression of oceanic anoxic event 1b in the North Atlantic, Sedimentology 58, 1217–1246.
924 Trecalli, A., Spangenberg, J., Adatte, T., Föllmi, K.B., Parente, M., 2012. Carbonate platform evidence
925 of ocean acidification at the onset of the early Toarcian oceanic anoxic event. Earth Planet. Sci.
926 Lett. 357–358, 214–225.

927 Twitchett, R.J., Krystyn, L., Baud, A., Wheeley, J.R., Richoz, S., 2004. Rapid marine recovery after the
928 end-Permian mass extinction event in the absence of marine anoxia. Geology 32, 805–808.
929 van de Schootbrugge, B., McArthur, J. M., Bailey, T. R., Rosenthal, Y., Wright, J. D. Miller K. G.,
930 2005. Toarcian oceanic anoxic event: An assessment of global causes using belemnite C isotope
931 records. Paleoceanography 20, PA3008.
932 Veizer, J., 1983. Chemical diagenesis of carbonates: theory and application of trace element technique.
933 SEPM Short Course Notes 10, 3.1–3.100.
934 Vörös, A., 1993. Jurassic brachiopods of the Bakony Mts. (Hungary): global and local effects on
935 changing diversity. In, Pálfy, J., Vörös, A. (Eds.), Mesozoic Brachiopods of Alpine Europe.
936 Hungarian Geological Society, Budapest, pp. 179–187.
937 Vörös, A., 2002. Victims of the Early Toarcian anoxic event: the radiation and extinction of Jurassic
938 Koninckinidae (Brachiopoda). Lethaia 35, 345–357.
939 Vörös, A., 2005. The smooth brachiopods of the Mediterranean Jurassic: refugees or invaders?
940 Palaeogeogr., Palaeoclimatol., Palaeoecol. 223, 222–242.
941 Vörös, A., Kocsis, Á.T., Pálfy, J., 2016. Demise of the last two spire-bearing brachiopod orders
942 (Spiriferinida and Athyridida) at the Toarcian (Early Jurassic) extinction event. Palaeogeogr.,
943 Palaeoclimatol., Palaeoecol. 457 233–241.
944 Ward, J.H., 1963. Hierarchical grouping to optimize an objective function, J. Am. Stat. Assoc. 58, 236–
945 244.
946 Wierzbowski, H., 2015. Seawater temperatures and carbon isotope variations in central European basins
947 at the Middle-Late Jurassic transition (Late Callovian-Early Kimmeridgian). Palaeogeogr.
948 Palaeoclimatol., Palaeocol. 440, 506–523.
949

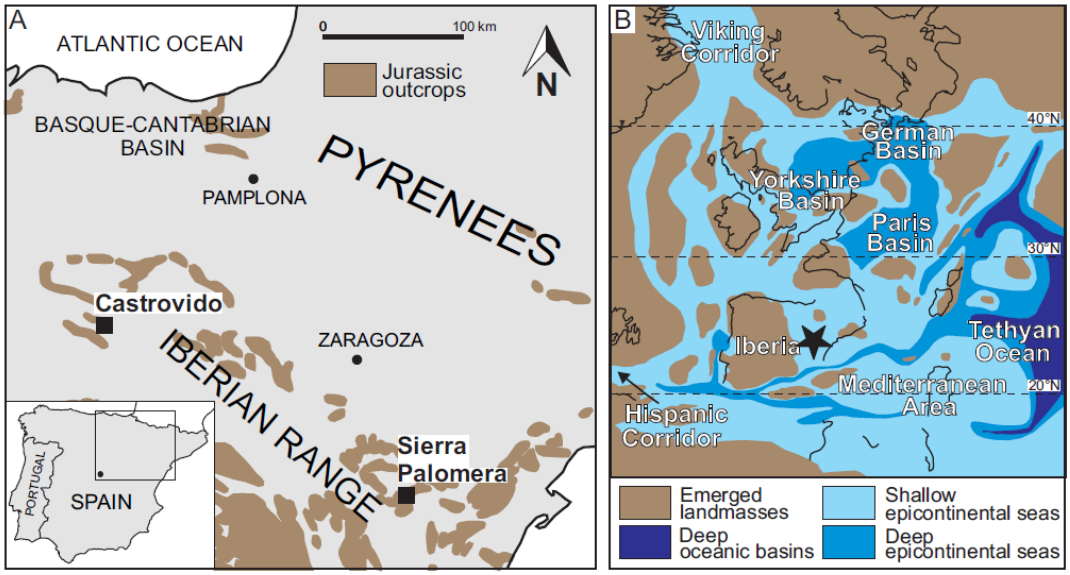

Fig. 1. Geographic location of the studied sections and early Toarcian palaeogeographic reconstruction of the NW Tethys. A, Location map showing the Castrovido and Sierra Palomera sections on the Iberian Range. Note that the system of shallow platforms deepened towards the N-NW, so that Sierra Palomera is in a shallower setting compared to Castrovido. B, Palaeogeographic reconstruction of the NW Tethys. Black star indicates the location of the system of shallow platforms now uplifted in the Iberian Range. A, Modified after Gómez and Goy (2011); B, modified after Dera et al. (2011).

950

951

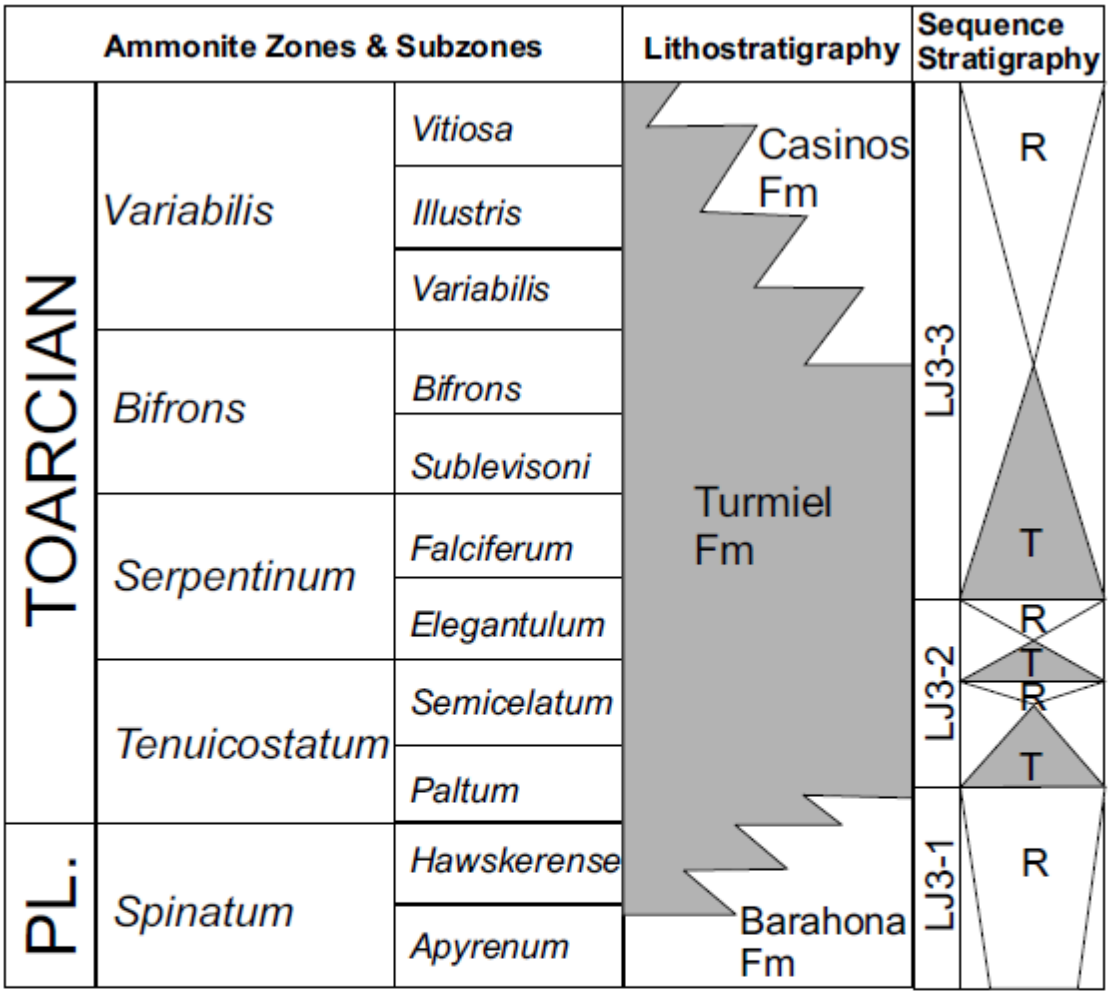

Fig. 2. Stratigraphic framework, including ammonite stratigraphy, lithostratigraphy and sequence stratigraphy, of the uppermost Pliensbachian – lower and middle Toarcian of the Iberian Range. Most of the lower Toarcian deposits are represented by an alternation of hemipelagic marls and lime mudstones of the Turmiel Formation. LJ3–1, LJ3–2, LJ3–3 represent third-order cycles within the upper Pliensbachian and the lower – middle Toarcian transgressive interval of the second-order cycle LJ-3. Abbreviations: PL., Pliensbachian. Modified after Gómez and Arias (2010).

952

953

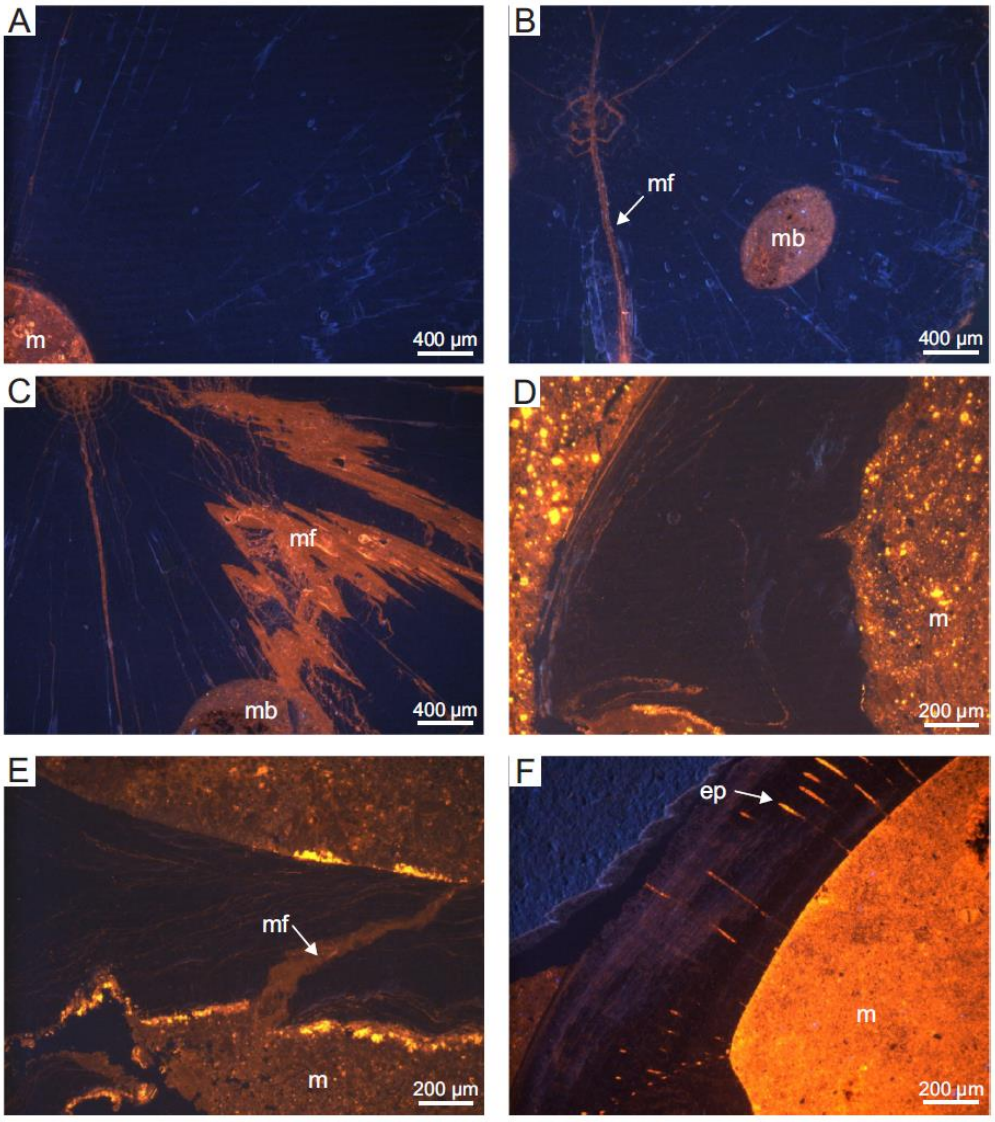

Fig. 3. Cathodoluminescence images showing different degrees of preservation of belemnites and brachiopods. A, Well preserved, non-luminescent, belemnite rostrum. Only exception is the apical canal, which is filled with matrix (m). B, Moderately well-preserved belemnite rostrum. Luminescence is low with the exception of a microfracture (mf) and a microboring (mb) filled, respectively, with secondary calcite and matrix. C, Diagenetically altered rostrum, with multiple and extensive microfractures, stylolites filled with highly luminescent calcite and the microboring filled with matrix. D, Well preserved, non-luminescent, rhynchonellid brachiopod shell in matrix. E, Well-preserved rhynchonellid brachiopod, with a microfracture filled with luminescent carbonate matrix. F, Moderately well-preserved (slightly luminescent) lobothyrid brachiopod shell, with endopunctae (ep) filled with carbonate matrix. Abbreviations: m, matrix; mf, microfractures; mb, microboring, ep, endopunctae.

954

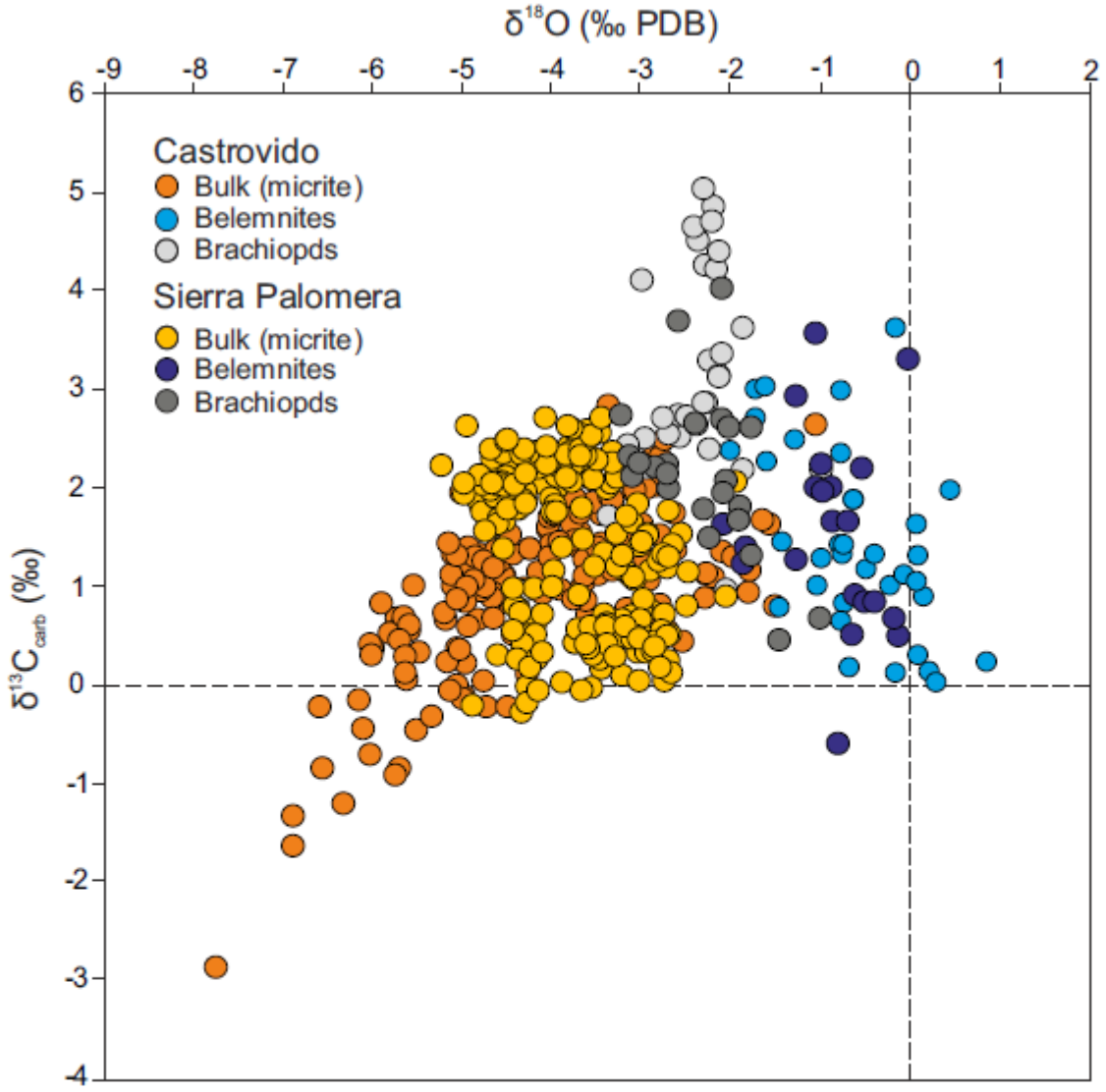

Fig. 4. Cross-plot of $\delta^{13}C$ and $\delta^{18}O$ data from bulk-rock samples, belemnites and brachiopod shells from Castrovido and Sierra Palomera. The linear trend towards very negative values ($\delta^{13}C < -1‰$; $\delta^{18}O < -6‰$) of some Castrovido bulk samples suggests a possible diagenetic overprint.

955

956

957

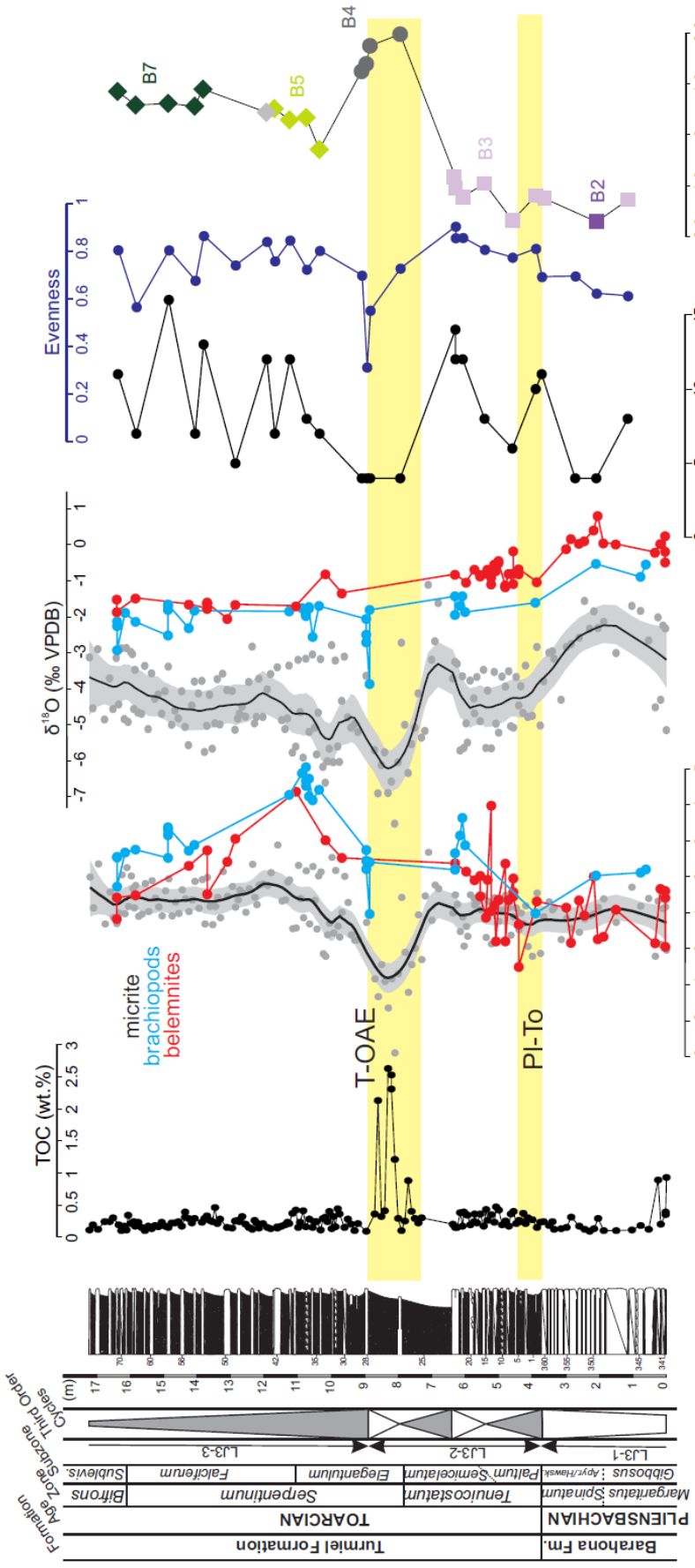

Fig. 5. Stratigraphy, geochemistry (TOC, $\delta^{13}C$, $\delta^{18}O$) and palaeoecology (Richness, Evenness, nMDS1) of the Pliensbachian-Toarcian section at Castrovido. Black lines represent the smoothed line (Loess smoothing factor 0.1) of the $\delta^{13}C$ and $\delta^{18}O$ bulk-sediment values (grey dots). Yellow boxes, defined by negative $\delta^{13}C_{micrite}$ excursions, indicate the Pliensbachian-Toarcian and early Toarcian CIEs. nMDS1 curve represents values of axis 1 of the nMDS ordination of Fig. 7A. Coloured dots on the nMDS1 curve represent different biofacies, as identified from the cluster analysis (see Fig. 8). Abbreviations: Pl-To: Pliensbachian-Toarcian; T-OAE: Toarcian Oceanic Anoxic Event. Lithostratigraphic units, ammonite zones, and transgressive-regressive cycles after Comas-Rengifo et al. (1988). (For interpretation of the references to colour in this figure legend, the reader is referred to the web version of this article.)

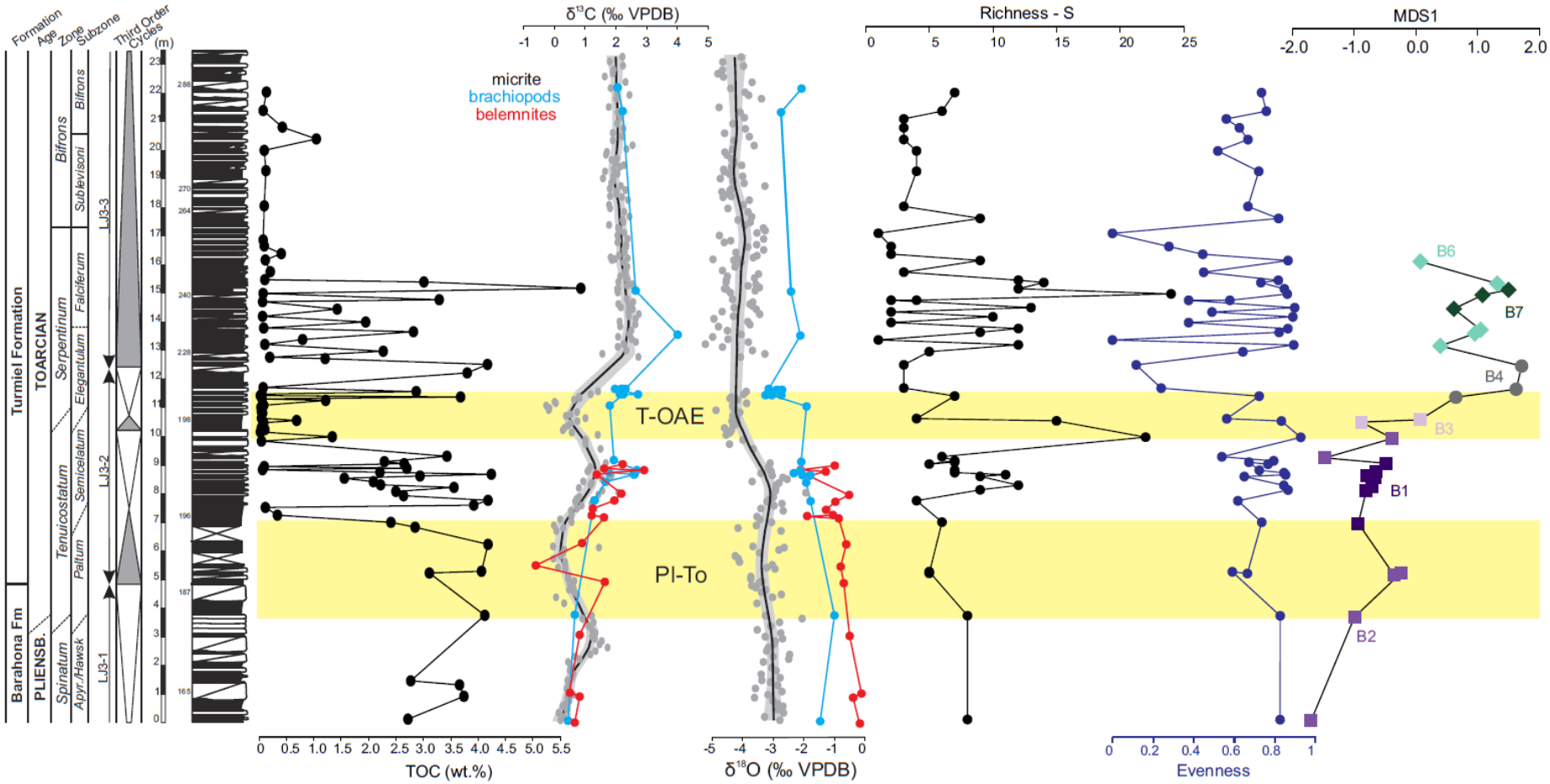

Fig. 6. Stratigraphy, geochemistry (TOC, $\delta^{13}C$, $\delta^{18}O$) and palaeoecology (Richness, Evenness, nMDS1) of the Pliensbachian-Toarcian section at Sierra Palomera. Black lines represent the smoothed line (Loess smoothing factor 0.1) of the $\delta^{13}C$ and $\delta^{18}O$ bulk-sediment values (grey dots). Yellow boxes, defined by negative $\delta^{13}C_{micrite}$ excursions, indicate the Pliensbachian-Toarcian and early Toarcian CIEs. nMDS1 curve represents values of axis 1 of the nMDS ordination of Fig. 7B. Coloured dots on the nMDS1 curve represent different biofacies, as identified from the cluster analysis (see Fig. 8). Abbreviations: Pl-To: Pliensbachian-Toarcian; T-OAE: Toarcian Oceanic Anoxic Event. Lithostratigraphic units, ammonite zones, and transgressive-regressive cycles after Comas-Rengifo et al. (1996). (For interpretation of the references to colour in this figure legend, the reader is referred to the web version of this article.)

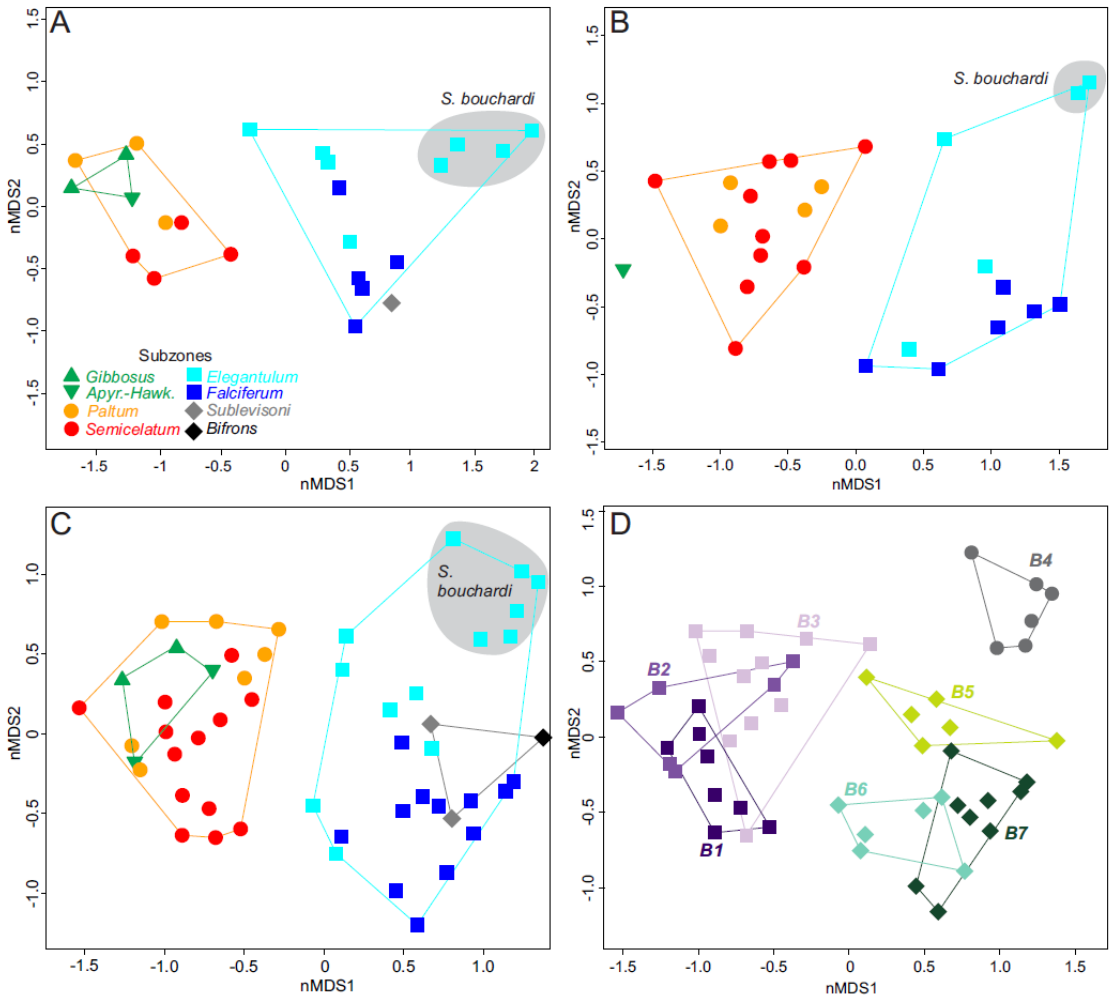

Fig. 7. Non-metric multidimensional scaling (nMDS) ordination of quantitative palaeoecological samples. A, Ordination of the dataset from Castrovido. B, Ordination of the dataset from Sierra Palomera. C, Ordination of the total dataset, which includes samples from both Castrovido and Sierra Palomera. In A, B, and C, samples are labelled according to the Subzone (legend in A); polygons group samples from the same ammonite zone. Grey area groups samples dominated by *Soaresirynchia bouchardi*. D, Ordination of the total dataset where samples are labelled according to the biofacies identified by the cluster analysis (Fig. 8, Table 1). Abbreviations: B1, *Gryphaea* cf. *sublobata* - *Plicatula spinosa* biofacies; B2, *Lobothyris* cf. *subpunctata* - *Pleuromya alduini* biofacies; B3, *Pseudopecten aequivalvis* - *L. arcta;* B4, *S. bouchardi* biofacies; B5, *Parvamussium pumilum* - *Homoeorhynchia batalleri* biofacies; B6, *Telothyris jauberti* - *T. pirenaica* biofacies; B7, *T. pirenaica* - *H. meridionalis* biofacies.

960

961

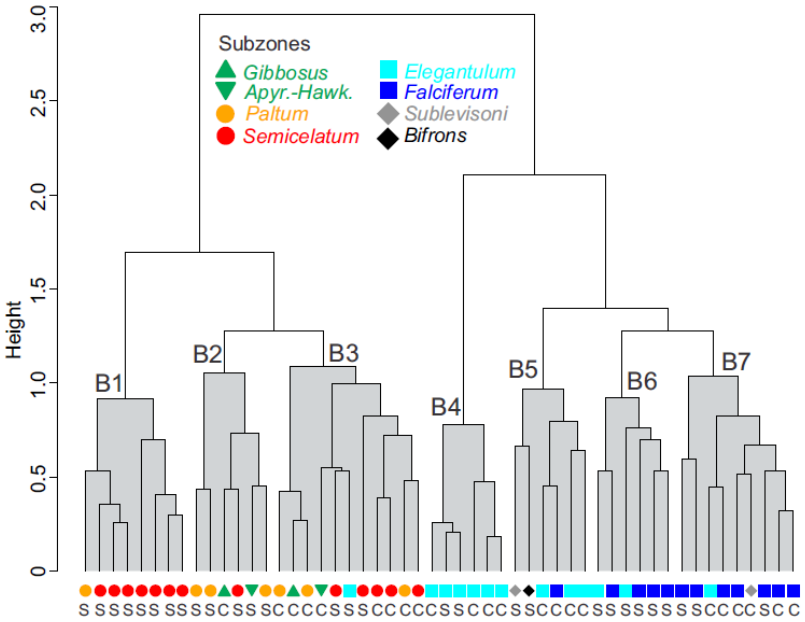

Fig. 8. Cluster analysis of the total palaeoecological dataset (Castrovido and Sierra Palomera together). Cluster analysis identified 7 groups of samples (coloured in grey) that have been interpreted as different benthic biofacies. Coloured symbols indicate the different ammonite subzones each sample belongs to. Abbreviations: C, Castrovido; S, Sierra Palomera.

962

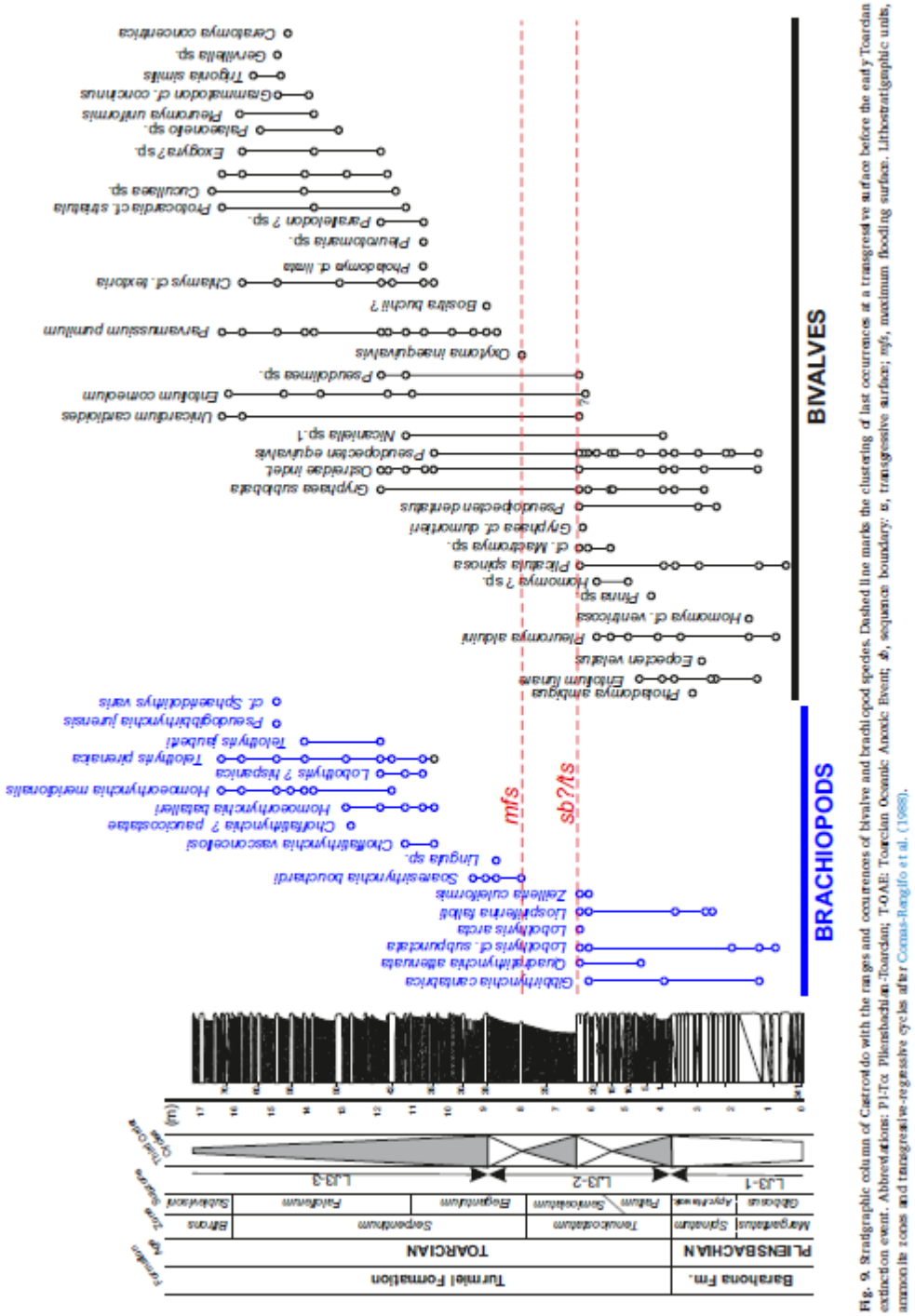

Fig. 9. Stratigraphic column of Castrotdo with the ranges and occurrences of bivalve and brachiopod species. Dashed line marks the clustering of last occurrences at a transgressive surface before the early Toarcian extinction event. Abbreviations: P-Tz Pliensbachian-Toarcian; T-OAE Toarcian Oceanic Anoxic Event; sb, sequence boundary: ts, transgressive surface; mfs, maximum flooding surface. Lithostratigraphic units, ammonite zones and transgressive-regressive cycles after Comas-Rengifo et al. (1988).

963

964

965

966

Table 1
Species composition of Pliensbachian-early Toarcian biofacies obtained with the cluster analysis on the total dataset (Fig. 8). Motility, tiering and feeding categories are shown for each species. Only species over 3% abundance are included. Abbreviations: FAC MOB: facultatively mobile; ST, stationary; EPI: epifaunal; D-INF: deep infaunal; INF: infaunal; SF: suspension feeder; GR: grazer; DF: deposit feeder; CARN: carnivore.

	%	Motility	Tiering	Feeding
B1				
Gryphaea cf. *sublobata*	36.8	ST	EPI	SF
Plicatula spinosa	15.0	ST	EPI	SF
Pseudopecten dentatus	10.7	FAC MOB	EPI	SF
Quadratirhynchia attenuata	7.7	ST	EPI	SF
Lobothyris arcta	4.7	ST	EPI	SF
Lobothyris cf. *subpunctata*	4.3	ST	EPI	SF
Plagiostoma subpunctatum	3.4	ST	EPI	SF
B2				
Lobothyris cf. *subpunctata*	34.1	ST	EPI	SF
Pleuromya alduini	24.4	FAC MOB	D-INF	SF
Gryphaea cf. *sublobata*	8.1	ST	EPI	SF
Zeilleria culeiformis	5.7	ST	EPI	SF
Pholadomya ambigua	4.9	FAC MOB	D-INF	SF
Pseudopecten aequivalvis	4.9	FAC MOB	EPI	SF
Ostreidae indet. 2	3.3	ST	EPI	SF
Plagiostoma subpunctatum	3.3	ST	EPI	SF
B3				
Pseudopecten aequivalvis	24.4	FAC MOB	EPI	SF
Lobothyris arcta	8.2	ST	EPI	SF
Gryphaea cf. *sublobata*	7.1	ST	EPI	SF
Lobothyris cf. *subpunctata*	6.8	ST	EPI	SF
Liospiriferina falloti	6.6	ST	EPI	SF
Plicatula spinosa	6.3	ST	EPI	SF
Lobothyiridae indet. 2	5.5	ST	EPI	SF
Pleuromya alduini	4.9	FAC MOB	D-INF	SF
Aulacothyris iberica	4.1	ST	EPI	SF
Ostreidae indet. 2	3.6	ST	EPI	SF
Mactromya sp.2	3.3	FAC MOB	INF	SF
B4				
Soaresirhynchia bouchardi	67.9	ST	EPI	SF
Parvamussium pumilum	14.6	FAC MOB	EPI	CARN
Plicatula auricula	9.4	ST	EPI	SF
Gryphaea crickleyensis	3.8	ST	EPI	SF
B5				
Parvamussium pumilum	20.0	FAC MOB	EPI	CARN
Homoeorhynchia batalleri	11.1	ST	EPI	SF
Telothyris pirenaica	10.0	ST	EPI	SF
Entolium corneolum	7.9	FAC MOB	EPI	SF
Chlamys textoria	7.4	FAC MOB	EPI	SF
Ostreidae indet. 2	5.8	ST	EPI	SF
Pseudolimea sp.	5.3	ST	EPI	SF
Pseudopecten aequivalvis	4.2	FAC MOB	EPI	SF

Table 2
Spearman's rank correlations between geochemical (TOC, $\delta^{13}C_{brac}$, $\delta^{18}O_{brac}$) and palaeoecological (Richness, Evenness, nMDS1) variables. In brackets, the number of observations (n) for each correlation. For each section, palaeoecological variables are measured for the total dataset, and for the bivalve and brachiopod dataset alone. In bold, correlations with $p < 0.05$.

	Castrovido			Sierra Palomera		
	TOC	δ^{13}Cbrac	δ^{18}Obrac	TOC	δ^{13}Cbrac	δ^{18}Obrac
S	−0.25 (n = 22)	0.31 (n = 13)	0.13 (n = 13)	**−0.41** (n = 43)**	0.23 (n = 12)	0.44 (n = 12)
S bivalves	−0.37 (n = 22)	0.19 (n = 13)	0.17 (n = 13)	**−0.50*** (n = 42)**	0.41 (n = 12)	0.36 (n = 12)
S brachiopods	−0.043 (n = 21)	0.43 (n = 13)	0.37 (n = 13)	−0.16 (n = 34)	0.01 (n = 12)	0.17 (n = 12)
Evenness	−0.12 (n = 22)	0.16 (n = 13)	0.18 (n = 13)	**−0.33* (n = 43)**	0.08 (n = 12)	0.36 (n = 12)
Evenness bivalves	−0.23 (n = 22)	0.019 (n = 13)	0.18 (n = 13)	**−0.45** (n = 42)**	0.29 (n = 12)	0.21 (n = 12)
Evenness brachiopods	−0.04 (n = 21)	0.42 (n = 13)	0.37 (n = 13)	−0.21 (n = 34)	−0.02 (n = 12)	0.07 (n = 12)
nMDS1	−0.4 (n = 20)	−0.48 (n = 13)	**−0.62* (n = 13)**	0.31 (n = 23)	−0.57 (n = 7)	−0.14 (n = 7)
nMDS1 bivalves	0.17 (n = 19)	−0.52 (n = 13)	**−0.61* (n = 13)**	0.24 (n = 21)	−0.54 (n = 6)	0.08 (n = 6)
nMDS1 brachiopods	0.24 (n = 11)	−0.092 (n = 9)	0.14 (n = 9)	−0.31 (n = 12)	0.1 (n = 5)	−0.5 (n = 5)

significance: $p < 0.05$: *, $p < 0.01$: **, $p < 0.001$: ***.